International Journal of Advanced Research in Engineering and Applied Sciences

ISSN: 2278-6252
Impact Factor: 5.795

BIOLOGICAL MODELING AS A MECHANICAL STUDY OF ALDEHYDES OXIDATION BY XANTINE OXIDASE ENZYME

Solomon Mulaw Sahle*

Prof. A.N. Mohamad**

Giday Gebregziabher Welegergs***

Haftu Gebretsadik Gebregziabher***

Abstract: *In the mechanism for purine metabolism the xanthenes oxidase enzyme has physiological importance. According to this hypothesis the xanthenes oxidase enzyme catalyzes the oxidation of xanthine to uric acid which plays a crucial role in gout, facilitate the reduction of oxidizing substrate and important for drug oxidation. Our calculation results indicate that in the catalysis stage the transition state is predicted in well tetrahedral complex formation with the strong bond formation of* $O_{eq} - C_{CRH}$ *and* $S_{Mo} - H_{RH}$ *, and the cleavage of* $C_{CRH} - H_{RH}$ *and* $Mo - O_{eq}$

This transition state is more reactant like, one imaginary negative frequency is performed and, high activation barriers are often obtained due to the absence of factors that stabilize the accumulation of charge on the substrate at the transition state. In this case the protonated aldehyde substrates more favored for the oxidation reaction with xanthine oxidase in comparison with the corresponding deprotenated aldehydes. And a step wise mechanism is found to be more favored for the oxidation of protonated formaldehyde with a proton coupled electron transfer and intermediate formation in the product bound. The result indicates that the enzyme xanthine oxidase is responsible for the oxidation of aldehydes based on the environment of the active site located. Our mechanistic study of the protonated formaldehyde oxidation provides an understanding in how the reaction path takes place and provides the way to study the catalytic mechanism on different oxidation substrates by xanthine oxidase enzyme.

Key words: *Molybdenum, homologies, hyperuricemia, nucleophilically attack and modeling of aldehyde family*

*Head of the Department of Chemistry, College of Natural and Computational Sciences, Debre Berhan University, Debre Berhan, Ethiopia

**Department of Mathematical Modeling, College of Natural and Computational Sciences, Debre Berhan University, Debre Berhan, Ethiopia,

***College of Natural and Computational Sciences, Debre Berhan University, Debre Berhan, Ethiopia

INTRODUCTION:

There are so many metals which are important biologically, one of the interesting and common uses in life is molybdenum, which serves as a cofactor for enzymes, we follow in this research survey of molybdo-enzymes; physiology and biochemistry of xanthine oxidase family enzymes; structure of xanthine oxidereductase; oxidation of aldehyde substrates by xanthine oxidase enzyme and using

MATERIALS:

Electronic structure calculations were performed using Gaussian 03W program soft ware package (Gaussian, Inc, Wallingford, CT) by applying density functional theory (DFT) method of the B3LYP correlation functional formalism (DFT – B3LYP). Including geometry optimization, frequency and linear transit calculations Gaussian view 3.0 (Gaussian inc. Pittsburg PA USA), a graphical user interface was used to prepare input files for Gaussian 03 it was also used to visualize the output files for Gaussian 03. Chem. Draw ultra chemical structure drawing standard version 8.0 (Cambridge soft corporation, Cambridge, MA USA) was used to build structures.

METHOD:

Predicting the transition state structure: The (DFT) method employing the B3LYP level of theory was applied on the truncated analogue of the reductive half reaction active site:

The truncated model structures were bound to respective forms of the substrates

Formaldehydes; Acetaldehyde; Propionaldehyde; Buthyraldehydes and Benzaldehyde we take **first three only** in this paper remaining will be done in future, through their HO_{eq} terminals. The 6 – 31G $(d^{'}, p^{'})$, basis set with a polarization function was applied for non metal atoms $(C, H, N \ and \ S)$. Similarly, the LANL2DZ basis set and LANL2 effective core potentials were applied for Mo atoms

SURVEY OF MOLYBDO – ENZYMES:

Enzymes that posse's molybdenum in their active sites catalyzes biological process that ate essential to the organism. The ability for molybdenum to exist in several oxidation states makes it suitable for biological electron transfer reaction coupled to oxygen atom or proton transfer [1]

Since the discovery of the first molybdenum enzyme, over 50 mononuclear molybdenum enzymes have been discovered [2]. They catalyze a variety of hydroxylation, oxygen atom

transfer, and other oxidation – reduction reactions, and share the unique molybdenum cofactor.

The mononuclear oxomolybdenum enzymes were divided into hydroxylases and oxotransferases due to the catalyzed reactions, the sequence homologies, and the comparison of the subunit and/or domain structures, the crystal structures as well as EPR and EZXAFS spectroscopic characteristics [3]. While hydroxylases are relatively homogenous group of enzymes with similar composition of cofactors and similar amino acid sulfoxide (DMSO) REDUCTASE AND sulfite – oxidase family. In the nitrogen cycle both molybdenum enzymes nitorgenase and nitrate reductase are key enzymes. In the metabolism of N – heterocyclic a large family of molybdenum enzymes encompasses a wide range of substrate specificities that allow hydroxylation of carbon centers in strategic regiospecificity. In the sulfur cycle, molybdenum dependent sulfite oxidation and dimethyl sulfoxide (DMSO) reduction play crucial roles. In carbon metabolism, both in the formation of methane and oxidation of format, carbon monoxide, and various aldehydes, the molybdenum enzymes again have a prominent position [1]

In prokaryotic organisms, the four most prevalent molybdenum containing enzymes are

a. Dimethyl sulfoxide reductase (DMSOR), which catalyzes the reduction of dimethyl sulfoxide to dimethlsulfide
b. Carbon monoxide dehydrogenize (CODH), which takes carbon monoxide to CO_2
c. Nitorgenase, with unique $MoFe7$ center that catalyzes the all important process of nitrogen fixation to form biovaluable ammonia and
d. Dissimilatory nitrate reductase, which catalyzes the reduction of $NO_3\ to\ N_2$, in autotrophic bacteria such that nitrate can be used as a terminal electron acceptor rather than O_2

The last group of respiratory enzymes involved in denitrification is found predominately in facultative anaerobes, and differ from the molybdenum containing assimilatory nitrate reductase that catalyze the conversion of nitrate to ammonium found in bacteria, fungi, and plants [4], [5]is found in three different enzymes:

Aldehyde oxidereductase (AOR), sulfite oxidase (SOX) and xanthine oxidereductase (XOR) Humans possess each of these enzymes, which differ slightly in the coordination of the molybdenum containing cofactor as shown in figure – 1: [2], [3]

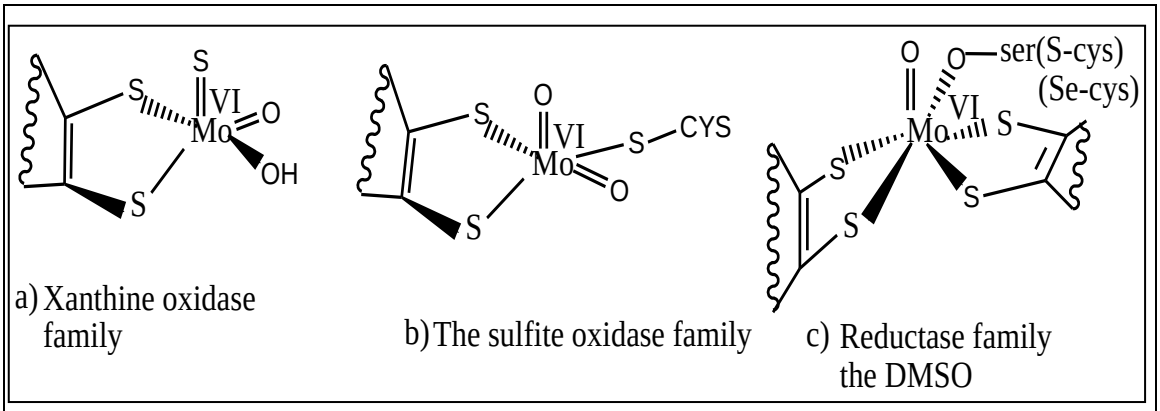

Figure 1: Structures of the reductive half-reaction active sites of the three families of mononuclear molybdenum enzymes. a) The xanthine oxidase family b) The sulfite oxidase family and c) The DMSO reductase family

The xanthine oxidase family includes those enzymes that catalyze oxidative hydroxylation reactions. Members of this family include the enzyme, for which it is named xanthine oxidase, as well as xanthine dehydrogenises aldehyde oxidase and CO dehydrogenize. The square pyramidal coordination sphere of Mo consists of an axial oxoligand, equatorial hydroxo and sulfide ligands, and the bidentate molybdopterin ligand (MPT). MPT is found in all monomolybdenum enzymes, and its role is to secure the metal to the protein, modulate the reduction potential and shuttle electrons between distant redox centers. And the molybdopterin (fig: 2) cofactor is a three ring structure composed of a pteridine nucleus fused to a pyran ring and attached to the molybdenum through a dithioline linkage [6]

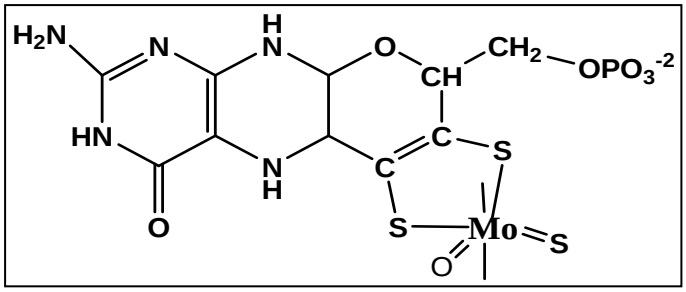

Figure 2: The molybdenum cofactor, Mo-co, comprising Mo legated to molybdopterin through the sulfur atoms of the dithioline group. The active, sulfo-form of the cofactor is shown.

The xanthine oxidase families have the same basic constitution of redox active centers:

Molybdenum center, two 2Fe/2S centers of the plant ferridoxin variety, and one flavin adenine dinileotide: The redox active centers of this enzyme are organized in a linear fashion ideal for electron transfer [7]. Electrons are passed into the molybdenum center from the substrate and then through FeS I, FeS II, and finally into the flavin center in the course of the reductive half reaction.

PHYSIOLOGICAL AND BIOCHEMISTRY OF XANTHINE OXIDASE FAMILY ENZYMES:

Xanthine oxidase (XO) is a molybdo falvoenzyme which can be found in almost all species, xanthine oxidereductase (XOR), first identified a century ago in milk, is highly conserved member of the molybdoenzyme family which also includes aldehyde oxidase (AO) and sulfide oxidase (SO) [8]. In mammalian organs, the highest level of XOR activity is express in liver [9]. Xanthine oxidereductase is a 290 kDa molybdenum containing enzyme that has been studied extensively from a biochemical perspective for more than 80 years [10]. The mammalian enzyme exists originally in the cell as the XDH form but is converted to the XO form by modification of the protein molecule. This conversion occurs either reversibly by oxidation of sufhydryl residues or irreversibly by proteolysis [11], [12]. XO is distributed in most of the tissues, with high levels in liver and intestine. Microscopic studies of cultured human endothelial cells showed that XO present in cytoplasm and also on the outer surface of the cell membrane [13]

Xanthine oxidase plays a key physiological role in the metabolism of purines which catalyses the hydroxylation reaction of hypoxanthine to xanthine, and subsequently xanthine to uric acid [3]

Increase in the production of uric acid or decrease in the excretion will lead to increase in the uric acid levels in the body. The increase of uric acid levels in blood is called hyperuricemia [14]

Hyperuricemea leads to man complications such as gout and kidney stones. It may also be associated with renal insufficiency and cardiovascular diseases

The name XOR describes an enzyme that exists in one of two forms, differing in respect to the preferred terminal electron acceptors. XOR is initially expressed as a dehydrogenize (XDH) that utilizes NAD^+, to produce NADH and it exists predominately in this form under physiological conditions [11], [12]. The enzyme can be converted to an oxidase XO by oxidation and/or limited proteolysis, a process that appear to be most prevalent in various pathologic states [15]. XO utilizes O_2, exclusively as its terminal electron acceptor and produces superoxide [7]. Another physiological role for XOR is in mammalian milk secretion. The enzyme has been shown to be membrane associated with milk fat globules as they are enveloped by apical cell membranes, and several studies suggest that its presence is necessary for proper secretion of milk during lactation [16]. The specific role of XOR is regards to

lactation remains unknown. XOR is found in virtually all cells throughout the human body, although its expression levels are highest in the hepatocytes, small intestinal enterocytes, and vascular endothelium [17]. It is a cytosolic enzyme, although some cells do exocytose the enzyme under certain physiological and pathological conditions. Aside from its role in normal purine catabolism, many other physiological functions have been proposed for the enzyme. One of these involves the production of nitric oxide from nitrate via reduction of NO_3^- *to* NO_2^- *and then to* NO. The following figure it is a hypothetical schematic model for the purine degradation pathway and ischemia reperfusion injury hypothesis.

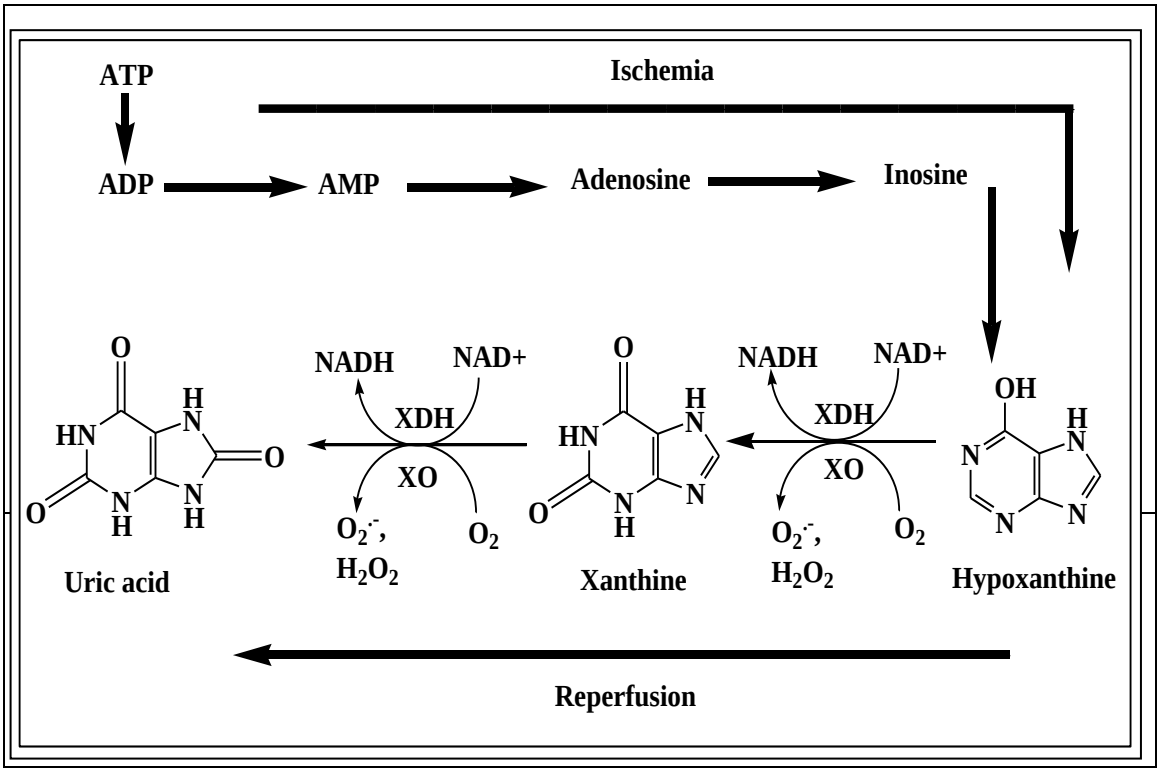

Figure – 3: A hypothetical Schematic model

STRUCTURE OF XANTHINE OXIDEREDUCTASE:

The early work on the structure of XOR was conducted by biophysical, chemical and spectroscopic methods, utilizing an ultraviolet visible absorbance, electrophoresis, and paramagnetic resonance techniques among others to elucidate the nature of the enzyme's structure and mechanism. In 1939, Prof. E.G. Ball showed that the yellow substance obtained following denaturation of isolated XOR was a flavin adenine dinulceotide similar to that isolated by Warburg and Christian from amino acid oxidase, thus indicating that the enzyme possessed an FAD cofactor [18]. This was the first redox active centers to be identified in the enzyme, although it was uncertain as to what role the FAD played in the function of XOR. Another redox active component of native XOR was identified in 1954 by D.A.Richert and

W.W.Westerfield, who demonstrated the requirement of iron in the functional enzyme, that making XOR an iron sulfur protein [6]. Xanthine oxidereductase contained molybdenum was elegantly and unequivocally demonstrated by Dr. R.C. Bray in 1966 with observation of a paramagnetic Mo (V) species in the enzyme [19]. Crystal structures of bovine enzyme were first determined separately by Ai – Nishino and Coworkers in 2000 [7], [20]

These studies provided direct assessment of the conclusions based on non crystallographic techniques. The bovine enzyme is a 290kDa homodimer, similar in molecular weight to the 275kDa homodimeric human enzyme. XOR from both sources contains one molybdenum atom site; two [2Fe – 2S] clusters positioned approximately 10Å away, and an FAD site where electrons are finally transferred out of the protein to a terminal electron acceptor. As mentioned, XOR exists as either XDH or XO, which preferentially utilize $NAD^+ over\ O_2$ respectively as the terminal electron acceptor from the flavin site. The specific preference of oxidizing substrates derives from the nature of the FAD site of the enzyme. XOR is initially expressed as XDH, but can undergo conversion to XO by oxidation of sufhydryl residues or by limited proteolysis around the flavin site, closing access to the site such that XO can utilize only molecular oxygen as its final electron acceptor [7]. Prior to this modification, XDH can use either electron acceptor, although it maintains a strong preference for NAD^+ , as given by the much lower K_d, for binding

$NAD^+ over\ O_2$, and a rate constant of NAD^+, reduction that is 5 to 10 folds greater than for O_2 reduction [21]; the catalytic sequence of XOR begins at the molybdenum site where electrons are introduced into the molybdenum cofactor, which is reduced from Mo VI to Mo IV [22]. Diagrammatically as shown in figure – 4: From there electrons are transferred one at a time to the more proximal of two [2Fe – 2S] clusters, positioned approximately 10 to 15 Å, away and each electron then moves approximately 8 to 10 Å, to the second cluster and finally each is passed 10 to 12 Å, to the FAD forming $FADH_2$ prior to reduction of the final exogenous oxidant. This sequence of intramolecular electron transfer occurs independently in each respective monomer, and it is not rate limiting catalysis by the enzyme [23]

The Reaction Mechanism of Xanthine Oxidase Enzyme:

The reaction of XO composed of two catalytic reactions, one is reductive half and other is the oxidative half reaction. The reductive half reaction is the conversion of xanthine to uric acid, which takes place in the molybdenum center of the enzyme. In this reaction, Mo VI is converted to its reduced form Mo IV. While the oxidative half reaction takes place at the

FAD center, and oxidize Mo IV to Mo VI by molecular oxygen with the formation of O_2^{*-} *or* H_2O_2 [24], [25]

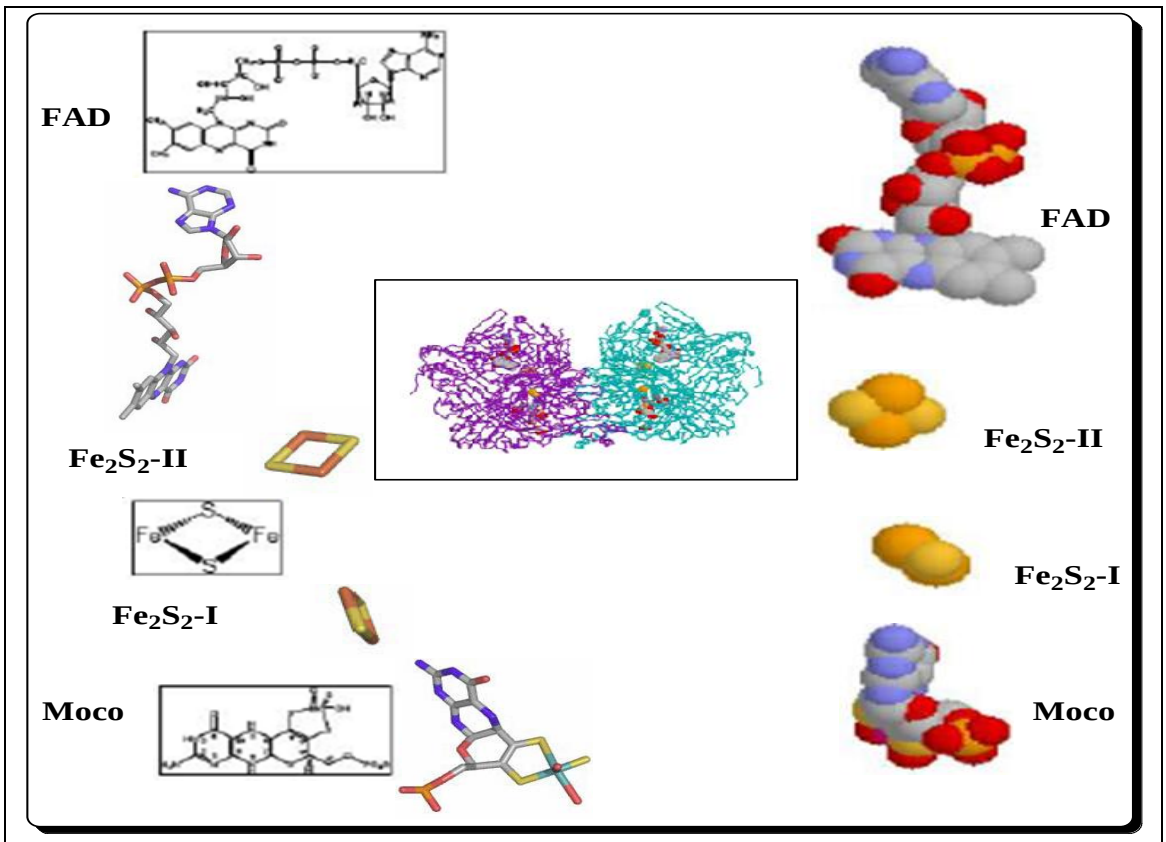

Figure 4: The overall structure (center) and cofactor compositions (left and right) of the ***bmXOR*** enzyme (PDB accession code of 10F4) [7]. Left and right display the linear arrangement of the cofactors: The FAD, pairs of [2Fe–2S], and Moco cofactors.

The oxidative part of the reaction involves the binding of molecular oxygen to the FAD center of the reduced form of XO. This will lead to the transfer of electrons from the reduced form, to achieve enzyme oxidation. Slow and fast phase in this reaction have been observed, and six electrons are transferred throughout the reaction [26]. The fast phase involves in the transfer of five electrons and the formation of hydrogen peroxide (H_2O_2) and superoxide (O_2^{*-}). Whereas the slow phase includes the oxidation of one electron and the formation of (O_2^{*-}) only [9]; the sequential scheme for the oxidative half reaction must therefore $6 \longrightarrow 4 \longrightarrow 2 \longrightarrow 1 \longrightarrow 0$,

Where the numbers reflect the number of reducing equivalents in each intermediate, a reason for the mechanism of the formation of xanthine and uric acid is considered as his reductive half reaction [27], schematic diagram as shown below in figure – 5 and 6:

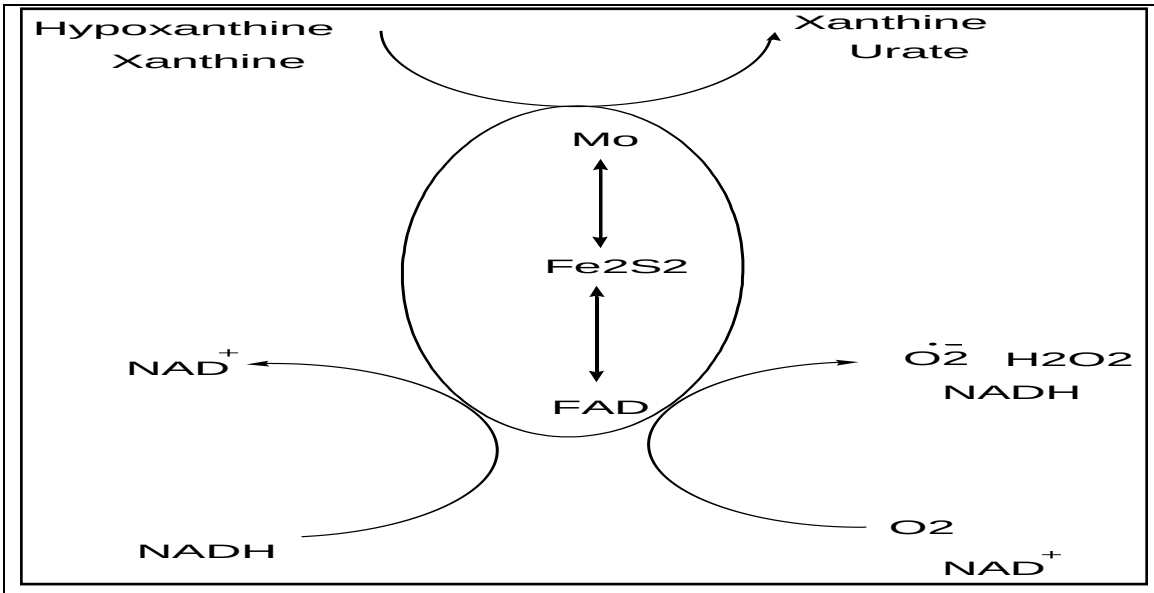

Figure 5: Schematic diagram showing XOR-catalyzed oxidation of xanthine and hypoxanthine (typifying most reducing substrates) at the Mo site, and of NADH at the FAD site. Reduction of NAD or molecular oxygen takes place at FAD.

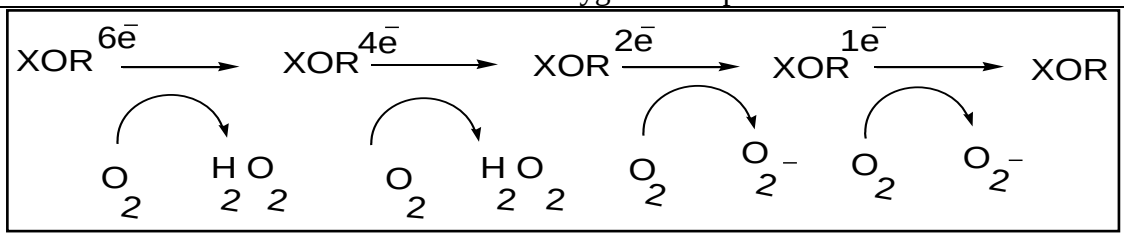

Figure 6: The oxidative half-reaction of xanthine oxidase. In the course of reoxidation of the enzyme ranging from 6 electrons reduced XO to fully oxidized XO.

Many researchers studied the catalytic reaction of XO proposing different mechanisms on the source and the way to incorporate the oxygen atom that is used to oxidize the substrate. But they all share the same concept, which is the hydroxylation to C8 of xanthine. In the early days of identifying the mechanism, it was proposed that the oxygen source is derived from water. However, it has been shown later that the oxygen atom incorporated into product is derived from the catalytically labile site of the enzyme, which must then be regenerated with oxygen from water. In addition, it has been suggested that the catalytically labile site of XO is in fact the

$Mo = O$, the enzyme as shown in figure – 6: the current mechanism for XOR enzymes.

It will be discussed detail here. It is currently believed that the glutamate 1261 residue acts as an active site base and initiates catalysis by abstracting the proton off the Mo – OH group. This enables the enzyme to nucleophilically attack the C8 proton to the sulfur on the molybdenum forming a Mo – SH and bringing about formal reduction of the molybdenum

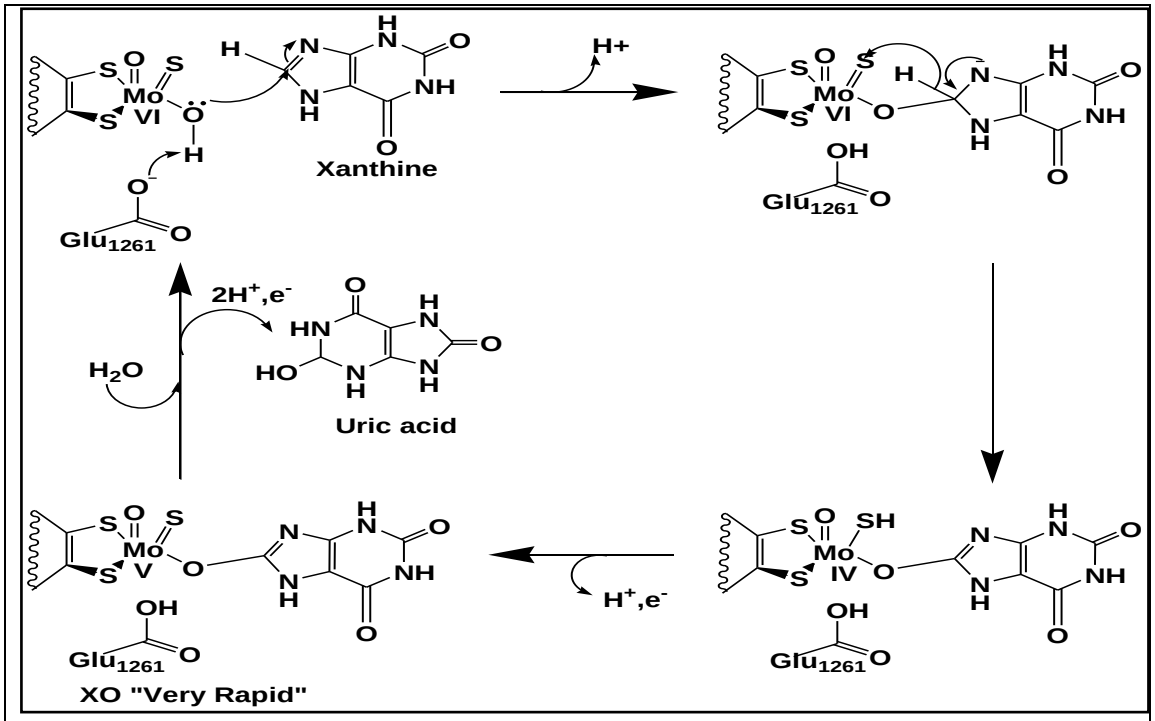

Figure 7: Postulated base-assisted hydride transfer mechanism for the hydroxylation of xanthine by XO enzyme. In the most favorable pathway, the [XOR]-Glu1261 is proposed to act as a general base.

The step is proposed to occur in one individual two electron step, forming a reduced enzyme product complex with Mo VI. One electron oxidation to form Mo V, along with deprotonation of the Mo=S species (with product still bound) yields the "very rapid" species observed by EPR. The product is then released via the rate limiting step, and the enzyme is oxidized and prepared for a second catalytic cycle [27]

This research was aimed on modeling a transition state structure for the transformation of **formaldehyde, acetaldehyde**, and **propylaldehyde** bound tetrahedral Michaelis – Menden type complex (MMTC) to the product bound intermediate. The mechanistic transformation of those simple aldehyde substrates bounded tetrahedral MMTS $\left((E_{OX}) - [Mo\,VI - O_{eq} - Csubstrate\right.$ to the product bound intermediate $EREDMo\ IVSMoHOeqCproduct$; it was passed through the tetrahedral transition state complex

$\left((E_{OX}) - [Mo\,VI - O_{eq} - C_{substrate}\ \ldots H_{RH} \ldots (= S_{Mo})]\right)$, the transition state structure was located in the presence of formaldehyde, acetaldehyde, and propylaldehyde and provide a more complete understanding of the events leading to the formation and decay of the transition state. And also the research was focused on probing a plausible mechanistic route

for the transformation of the formaldehyde bound tetrahedral MMTC to the product bound intermediate, either through a concerted or step wise oxidation processes. The transformation of a MMTC to the stable product bound intermediate is followed several paths, either concerted or step wise oxidation processes. We intend to use the electron density and charge analysis to support our hypothesis that the transformation is formaldehyde dependent and anticipate to takes place through a concerted or step wise oxidation processes. Note that the DFT method employing the B3LYP level of theory was applied on the truncated analogue of the reductive half reaction active site. The transition state was located for the transformation of those simple aldehyde substrates like formaldehyde, acetaldehyde, and propylaldehyde by plotting the graph energy (kcal/mole) versus S – H distance Å, and also one negative imaginary frequency was observed. Those all parameters were generated from geometry optimization, frequency and linear calculation, as shown below:

The aldehydes oxidation study is expected to provide additional insight into the reactions of XO family enzymes, by locating the transition state structure for the transformation of simple aldehyde substrates of aldehyde family bound tetrahedral MMTC to the product bound intermediate providing a more complete understanding of the events. In addition to this by applying an electron density and charge analysis like energy, Mullikan atomic charge and bond distance of selected atoms like molybdenum, hydrogen, carbon of the substance, sulfide terminal and oxygen can support our hypothesis

OXIDATION ALDEHYDE SUBSTRATES BY XANTHINE OXIDASE ENZYME:

Aldehyde features a sp^2 $hybridized$ planar carbon center that is connected by a double bond to oxygen and a single bond to hydrogen. The C – H bond is not acidic. Owing to resonance stabilization of the conjugate base, an $\alpha - hydrogen$, in an aldehyde is far more acidic with a $_{p}$Ka near 17 than a C – H bond in a typical alkane, with a $_{pKa}$ in the 30's.

This acidification is attributed to

a. The electron withdrawing quality of the formal center and
b. The fact that the conjugate base an emulate anion, delocalizes its negative charge

Related to (a), the aldehyde group is somewhat polar. These compounds are found at the most fundamental levels of biological existence. Aldehydes are more reactive than typical alkane; because when the pi – bond forms the electrons in this molecular orbital are more exposed, making them more vulnerable to reacting. The carbons of aldehyde are susceptible to both

oxidation and reduction and are easily oxidized to carboxylic acids. Some of the common simple aldehyde substrates are shown below in figure – 8:

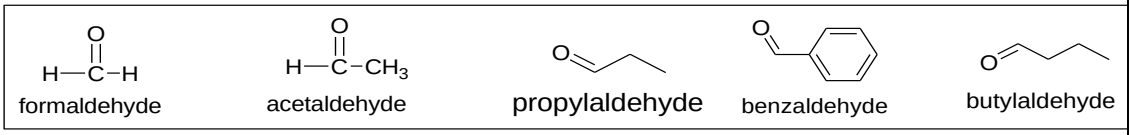

Figure 8: Structural representation of aldehyde substrates for the oxidation with xanthine oxidase enzyme.

Generally there are at least two distinct mechanisms by which one may envision the enzymatic oxidation of aldehydes. These involve the prior hydration of the aldehyde to a gem diol followed by the removal of a pair of hydrogen atoms or of a hydride ion plus a proton. The second mechanism proposes the removal of a hydride ion or its equivalent from the aldehyde and its ultimate replacement by a hydroxide ion from the medium as shown in figure – 7. To support our hypothesis that to probe the reaction path either concerted or step wise mechanism can relate with those several catalytic mechanisms which were proposed by different researches like Voittyuk et al [28], suggested a stepwise pathway based on a model density functional study. Theoretical studies using formaldehyde and form amide as substrates confirm that this process is concerted and occurs through tetrahedral arrangements around C8, these all supportive ideas as shown in schematic figure – 9.

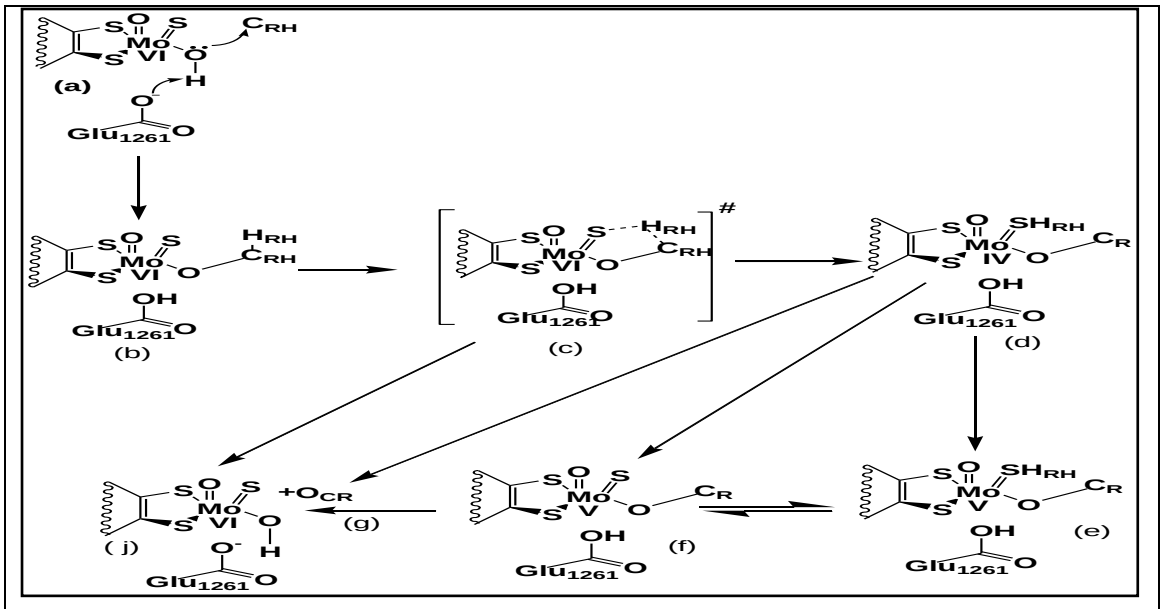

Figure – 9: A hypothetical schematic model for the catalytic transformation of the oxidation and hydroxylation of the substrate (C_{RH}) by XOR enzymes, in which C_{RH} is substituted by protonated and deprotenated formaldehyde, the major structural features for the meta-stable and transition state structures are shown.

From the above figure, at the transition state, several events are expected to take place, such as the transfer of H_{RH} , from formaldehyde carbon to the active site S_{Mo} terminal, concomitant transfer of two electrons to the Mo VI center, and conversion of the formaldehyde to product. The computational study performs an electronic structure calculations: Hence of this the data's gathered like energy, Mullikan atomic charge and bond distance approach to support our hypothesis as shown in (fig 9 c) it is dissociate into structure product release (j) with or without forming a stable intermediate product bind (d) up on this electron density and charge analysis, proposed catalytic mechanism and theoretical studies can expect that from the single point energy calculation, if there is a high energy barrier between the enzyme active site MOCO before bind the substrate formaldehyde (enzyme plus substrate) and the tetrahedral MMTC and between the two states in (fig 9) that stable intermediate is formed hence of that the reaction path way probe through stepwise and if the activation barrier is very much less or if the reaction path passes directly from the tetrahedral transition state complex to the product release (fig 9 g) without the formation of stable intermediate complex (fig 9 d) the reaction path way probe through concerted reaction mechanism

Geometrical representation of the transition state structures as shown below figure 10 – 12:

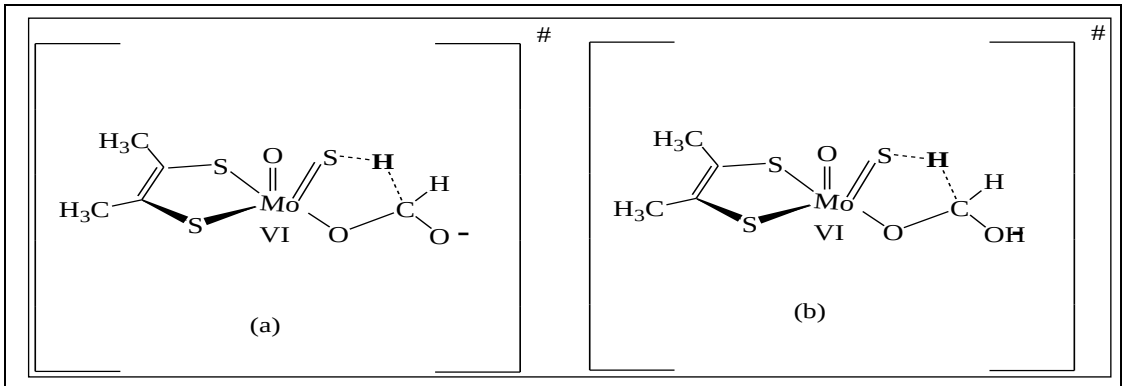

Figure 10: The geometries represent the transition state structures, modeling the Mo (VI) state of Moco bound to formaldehyde. The geometries were probed in (a) un protonated and (b) protonated conformations of the carbonyl oxygen of formaldehyde.

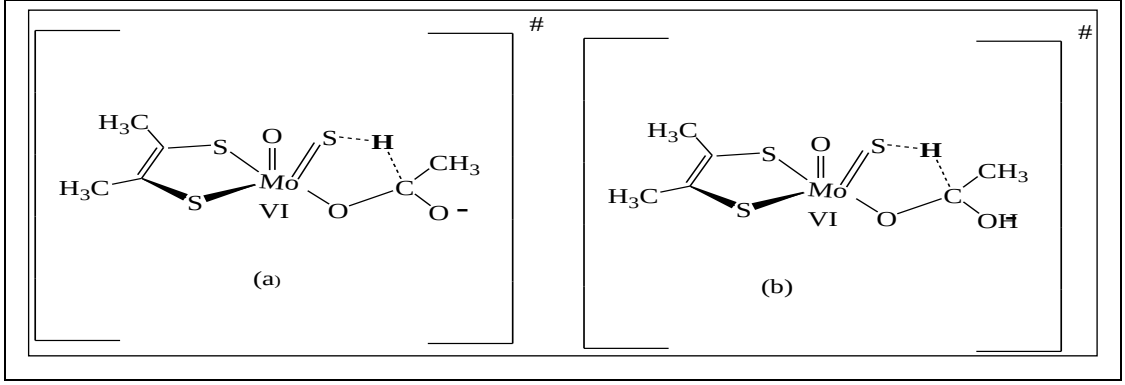

Figure 11.The geometries represent the transition state structures, modeling the Mo (VI) state of Moco bound to acetaldehyde. The geometries were probed in (a) un protonated and (b) protonated conformations of the carbonyl oxygen of acetaldehyde.

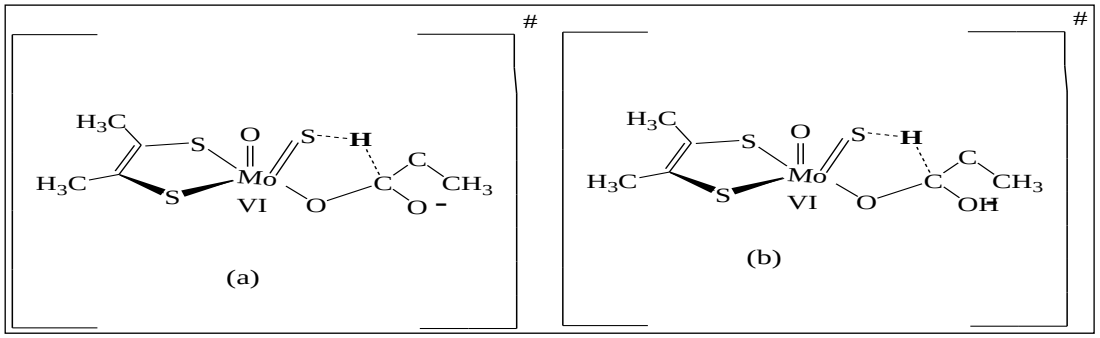

Figure 12: The geometries represent the transition state structures, modeling the Mo (VI) state of Moco bound to Propylaldehyde. The geometries were probed in (a) un protonated and (b) protonated conformations of the carbonyl oxygen of Propylaldehyde.

The transition state structure were determined using a linear motion of H_{RH}, during the migration of H_{RH} from C_{RH} to S_{Mo}, in which C_{RH} represents for the un protonated and protonated simple aldehydes like formaldehyde (fig 10) acetaldehyde (fig 11) propylaldehyde (fig 12). The scans were performed at the Mo IV and Mo IV states, respectively, representing the initial and final Meta stable structures, the total distance between H_{RH} and S_{Mo}, it was measured for all Mo –aldehyde complexes. But the net total distance covered byH_{RH}, it was calculated as taken the difference between total distances for $H_{RH} - (S \cdots H)$. Using the differences in distance with an interval $(0.1984, 0.16976), (0.1, 0.209), (0.1, 0.224107)$,of protonated and unprotonated formaldehyde, acetaldehyde, propylaldehyde respectively were used to construct the input files for linear transit calculations. The key word

"$\# \; opt = modredundant \; b31yp \; gen \; pseudo = read \;\; \# \; p \; gfinput \; iop \; (6/7 = 3) \; pop = full \; gfprint$"

The charge ad multiplicity $(-1, 1)$ and $(-2, 1)$, of the protonated and unprotonated aldehyde complexes were used for the linear transit calculation

The total energies from each optimization steps were plotted against respective H_{RH} and S_{Mo} distance from the plot the structure with the highest energy was considered as an initial guess for the transition state structure. The input files containing the three geometries (Initial, final and initial guesses) were optimized to generate the transition state structure. The key word "$\# \; b3LYP \; gen \; pseudo = read \;\; \# \; p \; gfinput \; iop \; (6/7 = 3) \; opt = qst3$"

It was used for transition state search. The output from transition state search was used as an input frequency calculation. From the frequency calculation the transition state was carried out by one imaginary negative frequency. Mullikan atomic charges on the selective groups

$(H_{RH}, C_{CRH}, Mo, O_{eq}\ and\ S_{Mo})$, collected to observe the charge variation and bond distance $(Mo - O_{eq}, H_{RH}, O_{eq} - C_{CRH}, C_{CRH} - H_{RH})$ They collected to approximate the weakening and strengthening of the bond. In addition to this from the collected Mullikan atomic charge, bond distance and energy a graph was plotted as energy versus S-H distance, charges versus S-H distance to observe the substrate with maximum energy and to indicate the inflection point respectively for the active site bound to simple aldehyde (Formaldehyde, acetaldehyde, and propylaldehyde)

PROBING THE REACTION MECHANISM:

As shown in figure – 13: A hypothetical schematic model for the catalytic transformation of the oxidation and hydroxylation of the substrate formaldehyde by XOR enzymes. The major structural features for the Meta – stable and transition state structures are shown. In order to probe the reaction mechanism, the events taking place before and after the transition (fig: 13) was investigated by applying electronic structure calculation. The complexes shown in (fig: 13) were optimized using key words

"$\sharp\ b3LYP\ gen\ pseudo = read\ \ \sharp\ p\ gfinput\ iop\ (6/7 = 3)\ opt\ pop = full\ gprint$"

The charge and multiplicity for the deprotenated formaldehyde (fig 13: – b, c, and d) respectively and for the Mo V substrate bound complex (fig 13: e and f) for $(-1, 2)\ and\ (-2, 2)$. The energy from each optimized structure was collected and calculated sing point energy $(Kcal/mole)$, versus reaction coordinate was plotted. The mechanism was probed from the evidence that related to the graph plotted at different energy barrier.

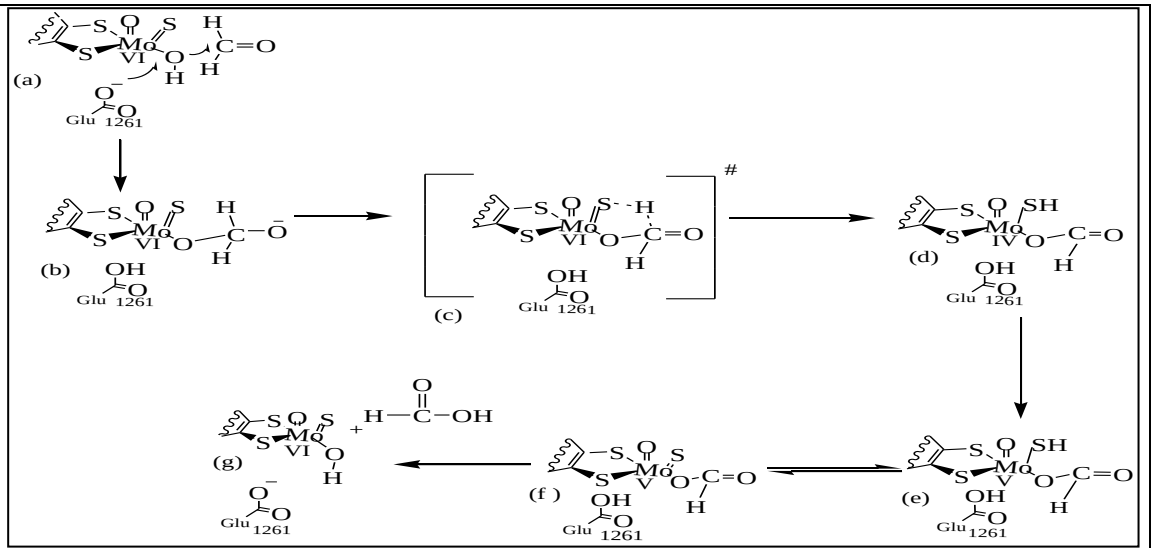

Figure 13: A hypothetical schematic model for the catalytic transformation of the oxidation and hydroxylation of the substrate formaldehyde by XOR enzymes. The major structural features for the meta-stable and transition state structures are shown.

Characterization of the transition state structure

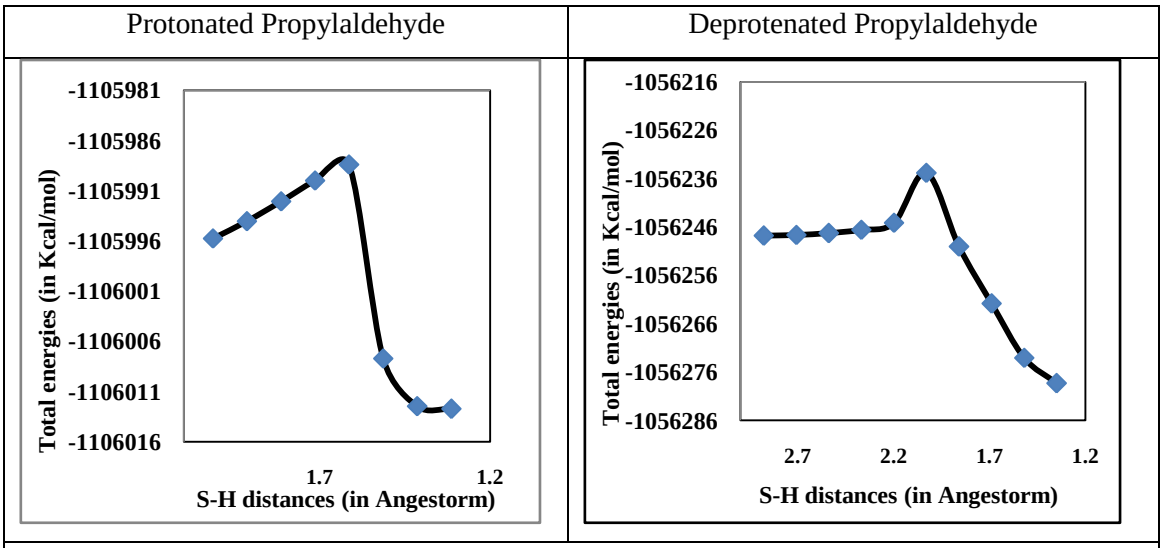

Figure 14: The graph obtained from the linear transit calculations for the truncated model Mo VI the active site bound to the protonated, deprotenated propylaldehyde structures shown in method (fig-10) in the migration of H_{RH} from C_{RH} to $\boldsymbol{S_{Mo}}$in the transition state structure. Graphs were plotted the total energies (in Kcal/mole) Vs $\boldsymbol{S_{Mo}}$-H_{RH} bond distances (in angstrom). The graphs were developed from the raw data provided in (Table Appendix I). The traces represent when H_{RH} was on C_{RH}-H_{RH} (left side) and $\boldsymbol{S_{Mo}}$-H_{RH} (right side).

The Change of the Mullikan atomic charges on$\left(\boldsymbol{H_{RH}, C_{CRH}, Mo, O_{eq}\ and\ OXO}\right)$, Sulfur back, Sulfur front and Sulfido groups

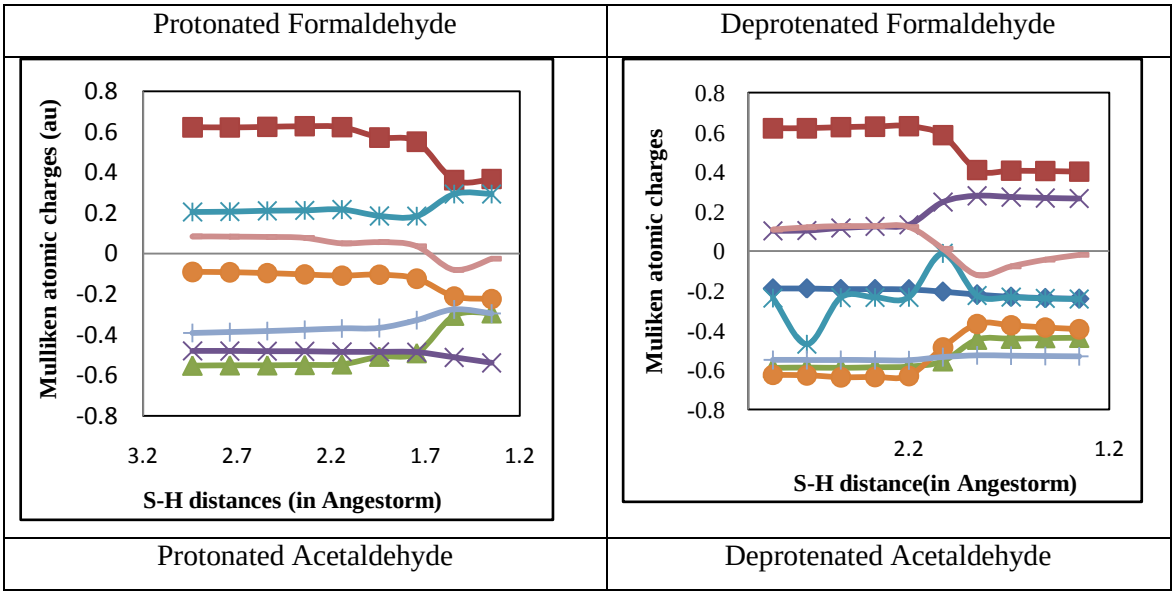

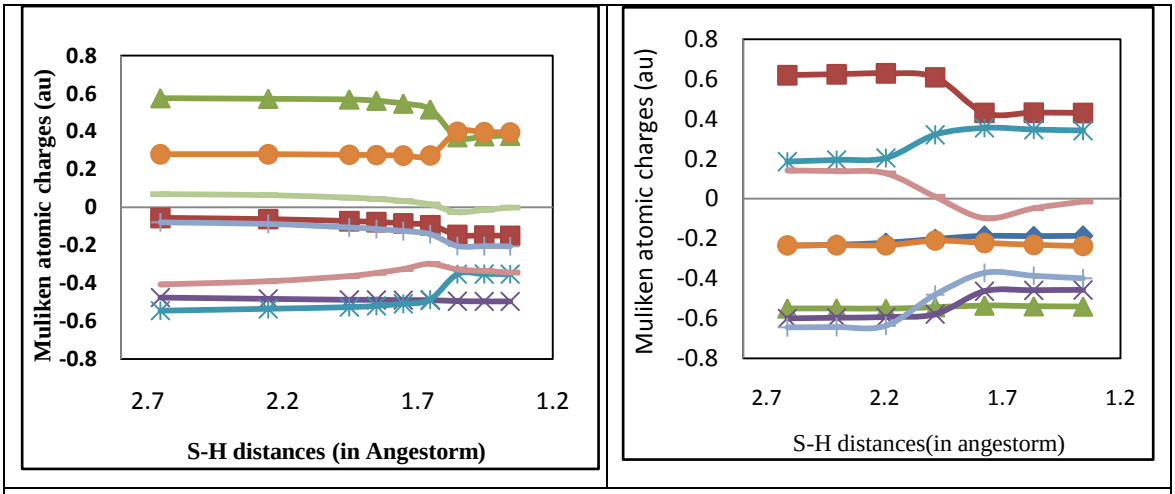

The traces from top to bottom represents Mo (first trace), C_{CRH} (second trace), H_{RH} (third trace), sulfur back (fourth trace), sulfur front (fifth trace), sulfide (sixth trace), O_{eq} (seventh trace) and OXO (eightieth trace)

Figure 15: The graph obtained from the linear transit calculations for the truncated model Mo (VI) the active site bound to the protonated, deprotenated formaldehyde and acetaldehyde in the migration of H_{RH} from C_{RH} to $\boldsymbol{S_{Mo}}$ in the transition state structure. Graphs were plotted the Mullikan atomic charges (au) Vs $\boldsymbol{S_{Mo}}$-H_{RH} bond distances (in angstrom). The graphs were developed from the raw data provided in (Table Appendix II).

Characterization of the normalized energy difference at C – H, TS and S – H bond Distances

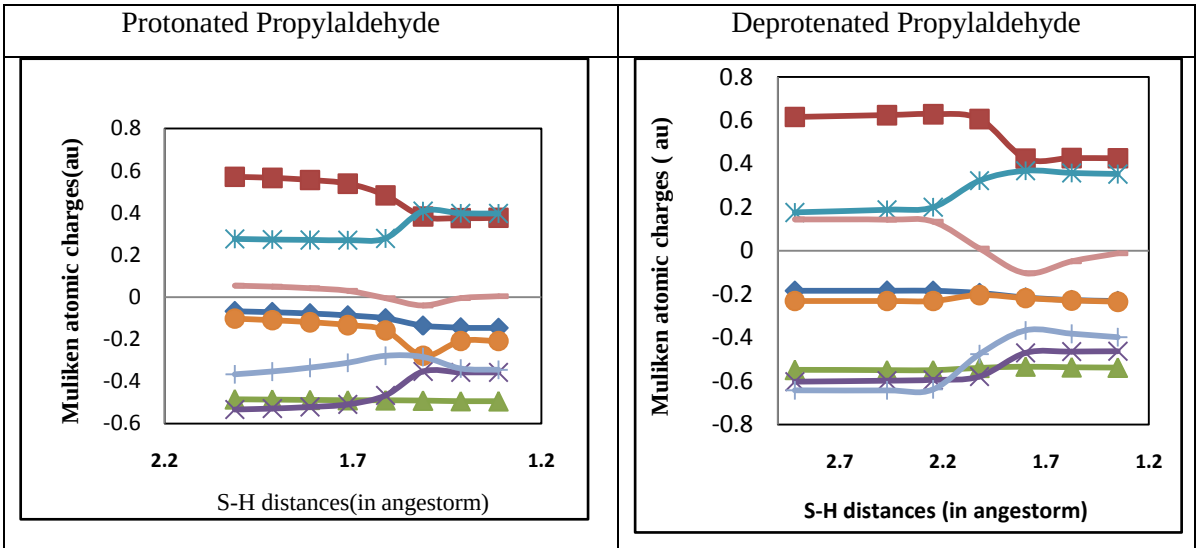

The traces from top to bottom represents Mo (1st trace), C_{CRH} (2nd trace), H_{RH} (3rd trace), sulfur back (4th trace), sulfur front (5th trace), sulfide (6th trace), O_{eq} (7th trace) and OXO (8th trace).

Figure 16: The graph obtained from the linear transit calculations for the truncated model Mo (VI) the active site bound to the protonated, deprotenated formaldehyde and acetaldehyde in the migration of $\boldsymbol{H_{RH}}$ from $\boldsymbol{C_{RH}}$ to $\boldsymbol{S_{Mo}}$ in the transition state structure. Graphs were plotted the Mullikan atomic charges (au) Vs $\boldsymbol{S_{Mo} - H_{RH}}$ bond distances (in angstrom). The graphs were developed from the raw data provided in Table Appendix II.

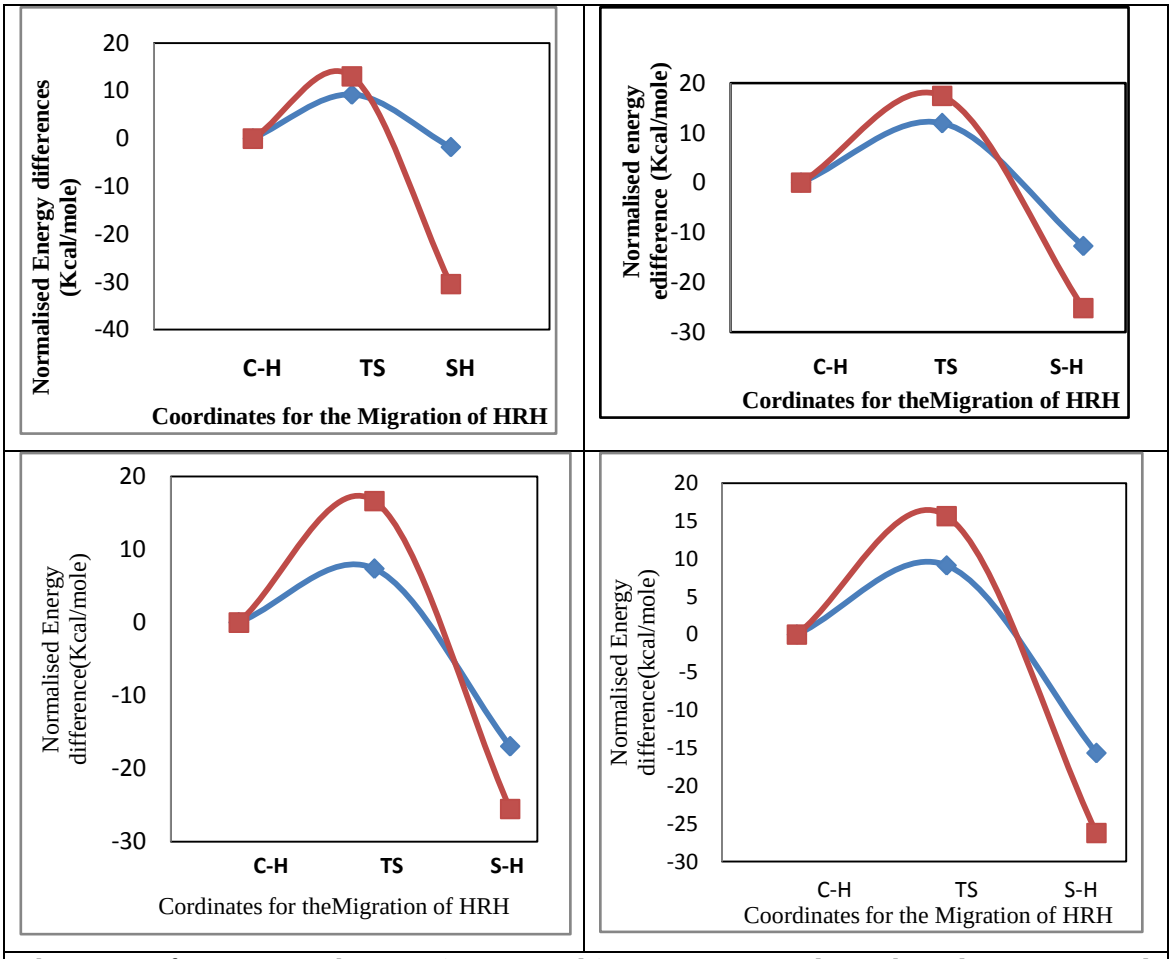

The traces from top to bottom (at S-H side) represent complexes bound to protonated formaldehyde, acetaldehyde, and propylaldehyde (1st trace) respectively and to deprotenated formaldehyde, acetaldehyde, and propylaldehyde (2nd trace) respectively.

Figure 17: The normalized energies, for the protonated and deprotenated formaldehyde, acetaldehyde, and propylaldehyde were plotted as a function of the reaction coordinates (C-H, TS, and S-H). The symbols (C-H, TS, and S-H) represent, respectively, the $\boldsymbol{MoVI-O_{eq}-C_{CRH}}$ meta-stable, transition ($[\boldsymbol{C_{CRH}\cdots H_{RH}\cdots SMo}]\ddagger$) and $\boldsymbol{MoVI-O_{eq}-C_{CR}-(-SH)}$) meta-stable states. The energy normalization was calculated with respect to the MMTC structure. $\boldsymbol{(MoVI-O_{eq}-C_{CRH}\text{meta}-\text{stable})}$, from the raw data provided in (Table Appendix. IV).

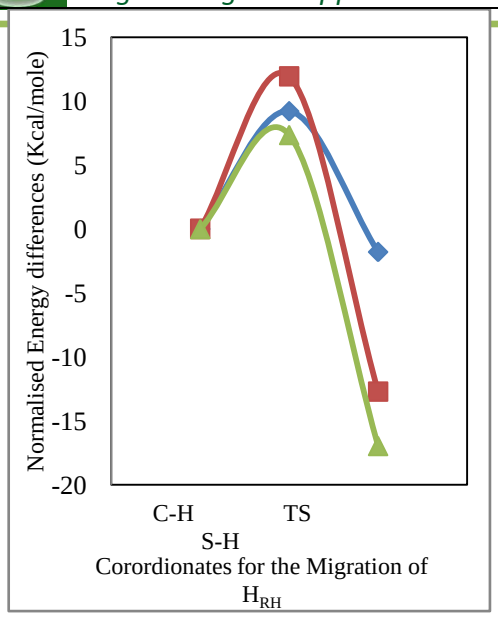

The traces for the transition state are as follows: top trace (Protonated acetaldehyde), 2nd trace (Protonated formaldehyde), and third trace (Protonated propylaldehyde)

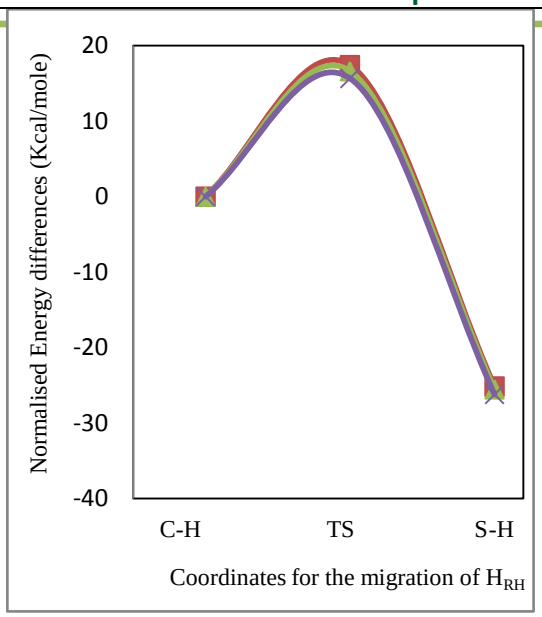

The traces for the transition state are as follows: top trace (deprotenated acetaldehyde), 2nd trace (deprotenated propylaldehyde and 3rd trace (deprotenated formaldehyde).

Figure 18: The normalized energies, for the protonated and deprotenated formaldehyde, acetaldehyde, and propylaldehyde were plotted as a function of the reaction coordinates (C-H, TS, and S-H). The symbols (C-H, TS, and S-H) represent, respectively, the $\boldsymbol{MoVI - O_{eq} - C_{CRH}}$ meta-stable, transition $([\boldsymbol{C_{CRH} \cdots H_{RH} \cdots SMo}]^{\ddagger})$, and $\boldsymbol{MoVI - O_{eq} - C_{CRH}(-SH)}$ meta-stable states. The energy normalization was calculated with respect to the Michaelis-Menden type structure $\boldsymbol{(MoVI - O_{eq} - C_{CRH}\text{meta} - \text{stable})}$ from the raw data provided in **(Table Appendix. IV)**

Characterization of the total energies $(\boldsymbol{Kcal/mole})$, at C – H, TS and S – H bond Distance in the linear transit Calculation

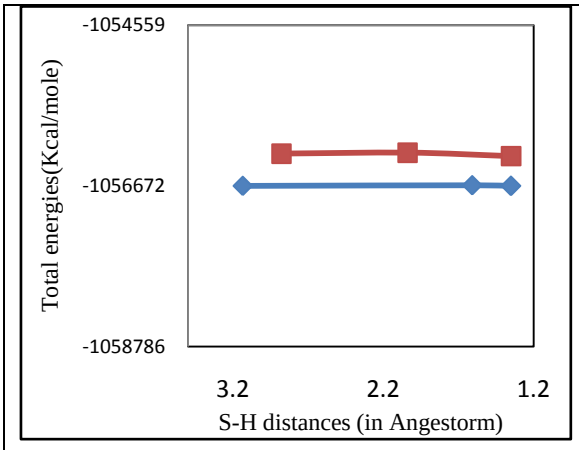

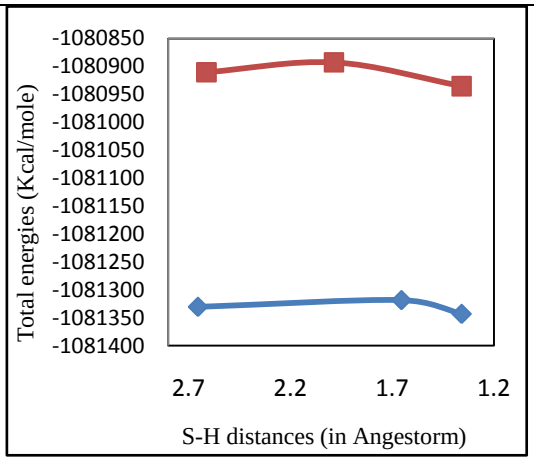

ISSN: 2278-6252
Impact Factor: 5.795

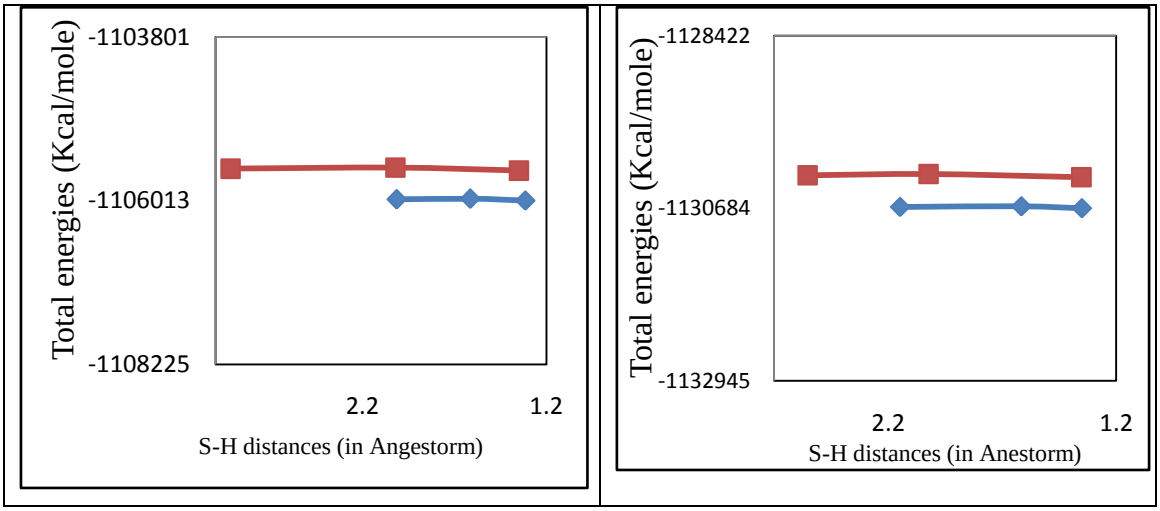

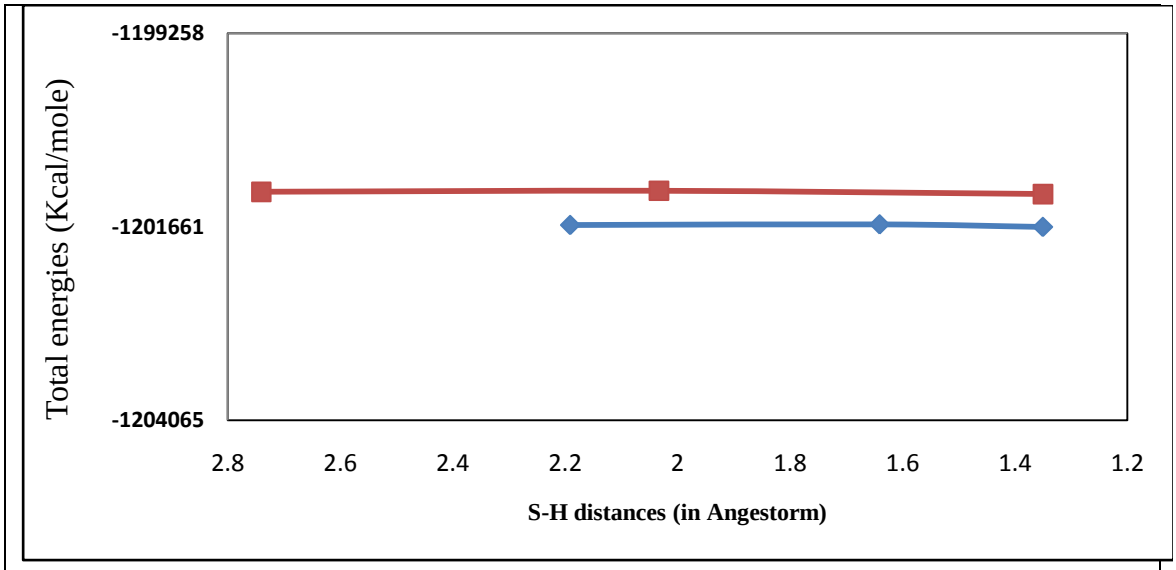

The traces from top to bottom (at S-H side) represent complexes bound to protonated formaldehyde, acetaldehyde, and propylaldehyde (2nd traces) respectively and to deprotenated formaldehyde, acetaldehyde, and propylaldehyde, (1st traces) respectively.

Figure 19: The total energies (in Kcal/mole), for the protonated and deprotenated formaldehyde, Acetaldehyde, propylaldehyde were plotted as a function of $S_{Mo} - H_{RH}$ bond distances (in angstrom) In the migration of H_{RH} from C_{RH} to S_{Mo} in the transition state structure: The total energy Difference was performed at C-H, TS and S-H: The graphs were developed from (Table Appendix. IV)

ISSN: 2278-6252
Impact Factor: 5.795

Characterization of Bond distances on $H_{RH}, C_{RH}, Mo, O_{eq}, OXO$, Sulfur back, Sulfur front and Sulfido groups in the linear transit calculation.

Protonated formaldehyde

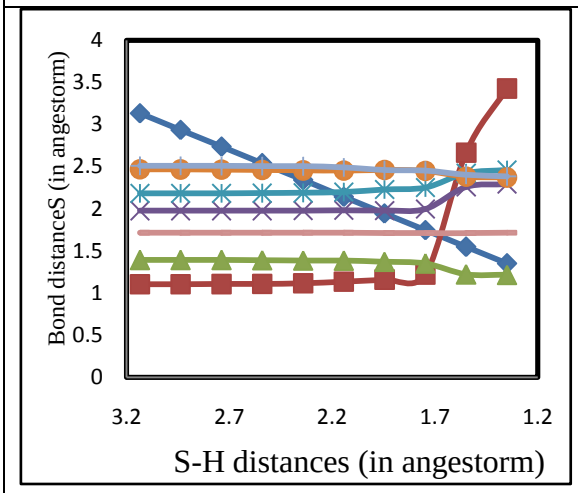

Deprotenated formaldehyde

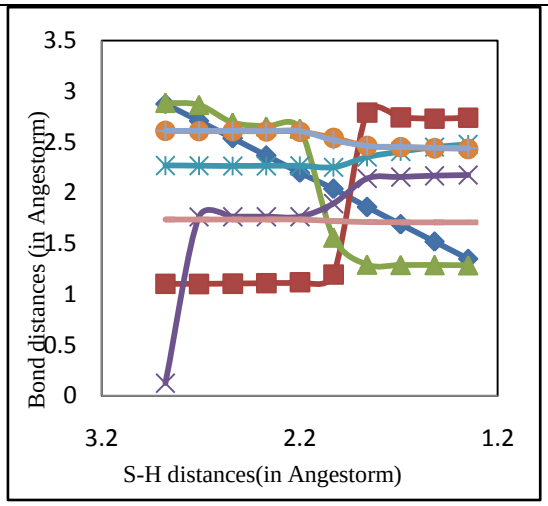

Protonated acetaldehyde

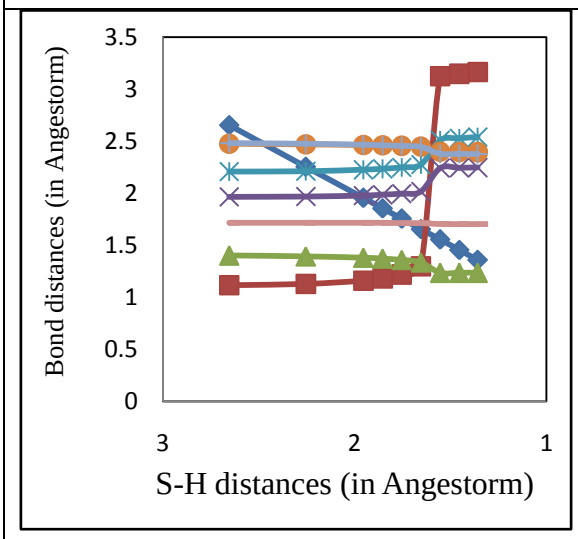

Deprotenated acetaldehyde

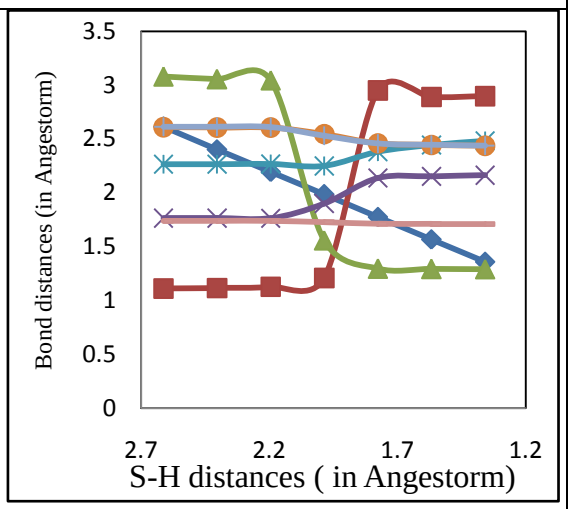

Figure 20: The graph obtained from the linear transit calculations for the truncated model Mo (VI) the active site bound to the protonated, deprotenated formaldehyde and acetaldehyde in the migration of H_{RH} *from* C_{RH} *to* S_{Mo} in the transition state structures. Graphs were plotted Bond distances (in Angstrom) Vs $S_{Mo} - H_{RH}$ bond distances (in angstrom). The graphs were developed from the raw data provided in (table A.III.1).

Probing the reaction mechanism for the hydroxylation of Protonated and deprotenated formaldehyde by xanthine oxidase enzyme

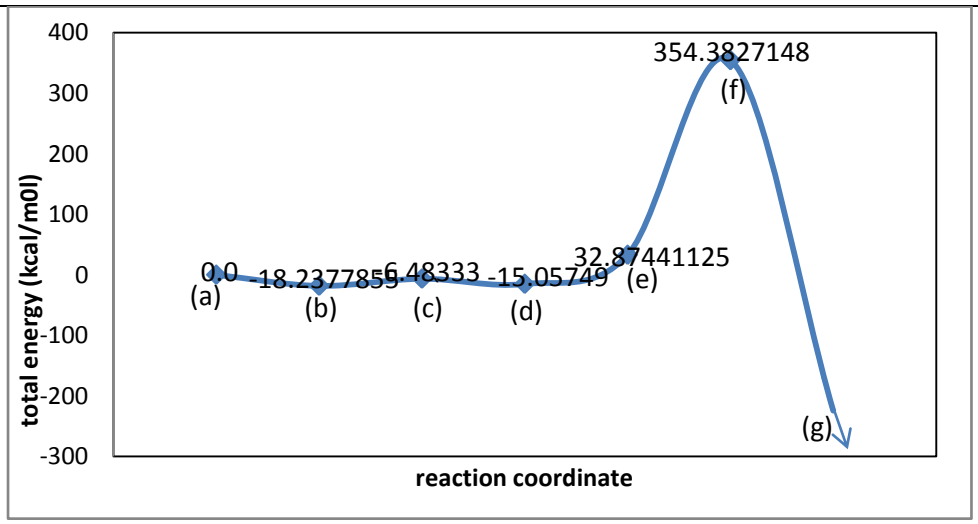

Figure 21: Calculated single-point energy profile for the reaction of Moco model, bound with protonated formaldehyde. The normalized single-point energies calculations are shown in parentheses. The calculations were performed for the truncated model of the active site bound to the protonated formaldehyde, as shown in figure 13: The geometries represents (a) the initial step (i.e. binding stage), (b) substrate bound type complex (c) the hypothetical tetrahedral transition state structure (d) product bound ***MoIV*** type complex,(e) product, the ***Mo V*** type complex, (f) ***Mo V*** rapid type complex, (g) represents the ***Mo VI*** complex results through a removal of one electron from the ***Mo V*** rapid type complex. the graphs were developed from the raw data provided in table A.V

.

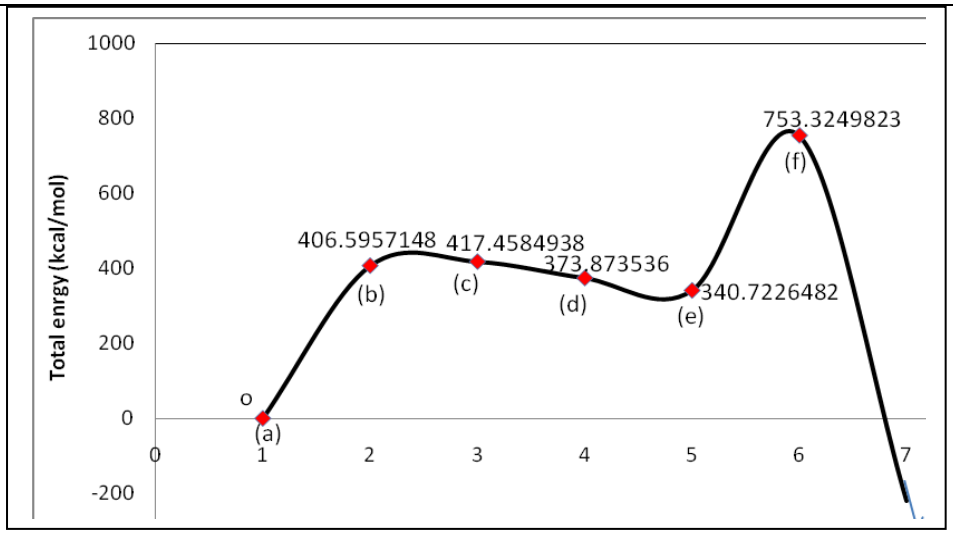

Figure 22: Calculated single-point energy profile for the reaction of Moco model, bound with deprotenated formaldehyde. The normalized single-point energies calculations are shown in (a) to (f). The calculations were performed for the truncated model of the active site bound to the deprotenated formaldehyde, as shown in the figure 13. The graphs were developed from the raw data provided in table A.V

CONCLUSION:

From the results of as above aspect we conclude that the xanthine oxidase has a physiological importance mechanically, biologically and medically in our environment, the main important thing is that for the oxidation of organic metabolites provides an understanding for their mechanic study. We plan to continue the judicious use of simple aldehyde molecules to aid in the interpretation of enzyme spectra and the determination of active site electronic structure. Computational methods were played as a master role in this research to elucidate the proposed mechanisms of oxidation of aldehydes. The frequency calculation the predicted transition state differs from other stationary points by one negative imaginary frequency. If anyone needs further deep works he can follow with help of negative imaginary frequencies. The potential energy for surface from the linear transit calculation also used to estimate the minimum energy required for the conversion of the substrate bound to product bound. The bond distance profiles at the catalysis phase were used to characterize the transition state. The Mullikan charge population profiles provided an evidence for the decreasing and increasing trends of the charge density. The mechanistic study for the oxidation of aldehydes by xanthine oxidase provides an understanding in the nature of the transition state and develops mechanistic study in the oxidation of protonated formaldehyde by xanthine oxidase. From the result obtained, like charge analysis and the activation barrier between each reaction coordinate the mechanism for the oxidation of protonated formaldehyde by xanthine oxidase enzyme is stepwise reaction.

Actually since this computational study in not an end for the mechanistic study of aldehydes oxidation by xanthine enzyme, having this can develop the mechanistic route for the deprotenated formaldehyde by clearly understanding the events leading for this problem and we will do with deprotenated and protonated of butyaldehyde and Benzaldehyde we will get further good results.

Appendix –I: The Raw Data used to characterize the Initial Stage

This raw data obtained from the linear transit calculation for Mo – VI state of Moco bound to protonated and Deprotenated formaldehyde, acetaldehyde and propylaldehyde respectively in the migration of $H_{RH}\ from\ C_{RH}\ to\ S_{Mo}$, And the total energies are shown from the$S_{Mo}\ to\ H_{RH}$ bond distance in angstrom

Protonated Formaldehyde		Deprotenated Formaldehyde		Protonated Acetaldehyde		Deprotenated Acetaldehyde	
S-H	Total Energy $(Kcal/mole)$	S-H	Total Energy $(Kcal/mole)$	S-H	Total Energy $(Kcal/mole)$	S-H	Total Energy $(Kcal/mole)$
3.1357	−1056670.443	2.87783	−1056 247.819	2.6544	−1081330.31	2.61239	−1080910.14
2.9373	−1056670.317	2.70807	−1056247.646	2.2544	−1081328.31	2.40339	−1080909.38
2.7389	−1056669.865	2.53831	−1056247.278	1.9544	−1081324.33	2.19439	−1080907.52
2.5405	−1056668.942	2.36855	−1056246.595	1.8544	−1081322.44	1.98539	−1080892.71
2.3421	−1056667.339	2.19879	−1056245.142	1.7544	−1081320.34	1.77637	−1080912.59
2.1437	−1056667.146	2.02903	−1056234.786	1.6544	−1081318.38	1.56737	−1080935.33
1.9453	−1056665.343	1.85927	−1056250.055	1.5544	−1081335.41	1.35837	−1080935.31
1.7469	−1056662.232	1.68951	−1056261829	1.3584	−1081343.03		

1.5485	−1056665.103	1.51975	−105637345				
1.3501	−1056672.242	1.34999	−1056278.305				

Protonated Propylaldehyde		Deprotenated Propylaldehyde	
S-H	Total Energy $(Kcal/mole)$	S-H	Total Energy $(Kcal/mole)$
2.0143	−1105995.76	2.9187	−1105581.793
1.9143	−1105994.045	2.4705	−1105581.136
1.8143	−1105992.061	2.2464	−1105579.593
1.7143	−1105989.981	2.0223	−1105565.163
1.6143	−1105988.400	1.7982	−1105583.102
1.5143	−1106007.702	1.5741	−115598.741
1.4143	−1106012.461	1.3500	−1105607.334
1.3143	−1106012.727		

This raw data obtained from the linear transit calculation for Mo – VI state of Moco bound to protonated and deprotenated formaldehyde, acetaldehyde and propylaldehyde respectively in the migration of $H_{RH}\ from\ C_{RH}\ to\ S_{Mo}$, and the total energies are shown from the$S_{Mo}\ to\ H_{RH}$ bond distance in angstrom

Appendix – II: The raw data for Mullikan atomic charges in the linear transit Calculation

Table – 2: The raw data for the Mullikan atomic charges for the following groups obtained from the linear transit calculation for *Mo–VI* state for Moco bound to protonated to deprotenated for the following in the migration of $H_{RH}\ from\ C_{RH}\ to\ S_{Mo}$

Deprotenated formaldehyde								
$S-H(\text{Å})$	Sulfur back	Mo	O_{OXO}	O_{eq}	C_{CRH}	Sulfur front	$Sulfido$	H_{RH}
2.87783	−0.188161	0.620721	−0.554942	−0.58880	0.102701	−0.236315	−0.62493	0.109216
2.70807	−0.188531	0.620730	−0.54967	−0.58822	0.104791	−0.469673	−0.62681	0.120401
2.53831	−0.191020	0.626651	−0.54968	−0.58919	0.117122	−0.234333	−0.63668	0.126490
2.36855	−0.191599	0.628868	−0.55000	−0.58656	0.124879	−0.233787	−0.63512	0.126133
2.19879	−0.193635	0.631387	−0.55093	−0.58283	0.133829	−0.232505	−0.63000	0.121256
2.02903	−0.204919	0.585977	−0.53490	−0.55590	0.248035	−0.011466	−0.48666	0.011339
1.85927	−0.219858	0.409394	−0.52568	−0.44708	0.279906	−0.223389	−0.36744	−0.12112
1.68951	−0.23035	0.406647	−0.52801	−0.44201	0.273288	−0.232139	−0.37444	−0.07739
1.51975	−0.236948	0.405328	−0.52858	−0.43857	0.268389	−0.238323	−0.38499	−0.04309
1.34999	−0.239877	0.401858	−0.53046	−0.43691	0.265808	−0.241782	−0.39418	−0.01875
Protonated formaldehyde								
$S-H(\text{Å})$	Sulfur back	Mo	O_{OXO}	O_{eq}	C_{CRH}	Sulfur front	Sulfido	H_{RH}
3.1357	−0.064406	0.624014	−0.551346	−0.478539	0.203496	−0.089046	−0.3954	0.083384
2.9373	−0.06951	0.632481	−0.548361	−0.480102	0.203092	−0.090382	−0.4008	0.078669
2.7389	−0.067433	0.619308	−0.542473	−0.476035	0.199122	−0.106819	−0.3911	0.065098
2.5405	−0.085237	0.629931	−0.534971	−0.475155	0.199543	−0.112929	−0.3825	0.046760
2.3421	−0.109662	0.644161	−0.524604	−0.474130	0.196386	−0.119143	−0.3669	0.026598
2.1437	−0.139056	0.659248	−0.511210	−0.473084	0.184707	−0.1224666	−0.3418	0.009861
1.9453	−0.172646	0.670859	−0.496567	−0.472561	0.164319	−0.124797	−0.3068	0.002679
1.7469	−0.208313	0.674973	−0.484074	−0.472759	0.152855	−0.126814	−0.2687	0.007870
1.5485	−0.241050	0.676916	−0.476504	−0.472912	0.130904	−0.127657	−0.2432	0.018380
1.3501	−0.267559	0.683973	−0.473380	−0.472362	0.128472	−0.127159	−0.2357	0.027540
protonated acetaldehyde								
$S-H(\text{Å})$	Sulfur back	Mo	O_{OXO}	O_{eq}	C_{CRH}	Sulfur front	Sulfido	H_{RH}
1.35837	−0.185733	0.43036	−0.5393	−0.4571	0.34197	−0.235898	−0.3995	−0.013786
1.56737	−0.186180	0.43198	−0.5379	−0.4588	0.34678	−0.230928	−0.3860	−0.046977
1.77637	−0.185964	0.43072	−0.5351	−0.4634	0.35587	−0.221162	−0.3711	−0.097703
1.98539	−0.201214	0.60854	−0.5430	−0.5784	0.32098	−0.209553	−0.4808	0.010651
2.19439	−0.220116	0.62919	−0.5504	−0.5923	0.20429	−0.232971	−0.6360	0.128097
2.40339	−0.230663	0.62442	−0.5500	−0.5958	0.19486	−0.232558	−0.6427	0.138241
2.61239	−0.235127	0.61952	−0.5498	−0.5987	0.18657	−0.233539	−0.6442	0.142175
Protonated acetaldehyde								
$S-H(\text{Å})$	Sulfur back	Mo	O_{OXO}	O_{eq}	C_{CRH}	Sulfur front	Sulfido	H_{RH}
2.65438	−0.55821	0.576383	−0.47480	0.54435	0.280358	−0.078629	−0.405922	0.069876
2.25438	−0.061909	0.573420	−0.48158	0.53512	0.280217	−0.087086	−0.389547	0.064517
1.95438	−0.072227	0.570213	−0.48624	0.52534	0.278096	−0.104810	−0.360042	0.051559
1.85438	−0.077686	0.563410	−0.48739	0.51915	0.275985	−0.113752	−0.346086	0.044366
1.75438	−0.084494	0.547932	−048834	0.50805	0.273486	−0.124633	−0.325124	0.034181
1.65438	−0.094363	0.517055	−0.48915	0.48585	0.273916	−0.141042	−0.297231	0.015570
1.55438	−0.144965	0.370748	−0.49447	0.35121	0.398820	−0.203535	−0.326778	−0.02538
1.45438	−0.147634	0.375472	−0.49513	0.35120	0.397001	−0.2014126	−0.335419	−0.01208
1.35837	−0.149063	0.378199	−0.49544	0.35130	0.395718	−0.204465	−0.342869	−0.00131
Deprotenated propylaldehyde								
$S-H(\text{Å})$	Sulfur back	Mo	O_{OXO}	O_{eq}	C_{CRH}	Sulfur front	Sulfido	H_{RH}
2.918748	−0.184287	0.615043	−0.54929	−0.60223	0.175475	−0.232090	−0.64258	0.143799
2.470534	−0.185009	0.623319	−0.54941	−0.59853	0.188452	−0.231396	−0.64302	0.142988

2.246427	−0.184863	0.628130	−0.54982	−0.59487	0.200085	−0.231521	−0.63811	0.133391
2.022320	−0.194949	0.605710	−0.53991	−0.57889	0.322754	−0.204397	−0.47621	0.009064
1.798213	−0.215159	0.423988	−0.53394	−0.47015	0.368292	−0.218758	−0.36678	−0.10416
1.574106	−0.227017	0.426225	−0.53733	−0.46463	0.357856	−0.229463	−0.38270	−0.04861
1.349999	−0.231916	0.425749	−0.53885	−0.46272	0.352559	−0.235223	−0.39772	−0.01297
Protonated propylaldehyde								
$S-H(\text{Å})$	Sulfur back	Mo	O_{OXO}	O_{eq}	C_{CRH}	Sulfur front	Sulfido	H_{RH}
2.01439	−0.06782	0.570702	−0.48569	−0.53376	0.27629	−0.10155	−0.36652	0.054801
1.91439	−0.07223	0.565593	−0.48701	−0.52875	0.273677	−0.10922	−0.35340	0.049603
1.81439	−0.07822	0.556018	−0.48811	−0.52156	0.271111	−0.11932	−0.33526	0.041835
1.71439	−0.08635	0.538450	−0.48893	−0.50910	0.269772	−0.13300	−0.31168	0.029361
1.61439	−0.10058	0.482557	−0.49015	−0.46654	0.278553	−0.15780	−0.27858	−0.00477
1.51439	−0.13535	0.382350	−0.49176	−0.35290	0.407409	−0.27848	−0.28395	−0.03949
1.41439	−0.14535	0.374591	−0.49418	−0.35676	0.398169	−0.20795	−0.33853	−0.00578
1.31439	−0.14639	0.376242	−0.49442	−0.35684	0.397108	−0.20818	−0.34509	−0.00392

Appendix –I II: The raw data for bond distance in the catalysis stage

Table – 3: The raw data for the bond distance for the following groups. The calculations were performed for MO VI state Moco bound to deprotenated and protonated formaldehyde, acetaldehyde and propylaldehyde in the migration of $H_{RH}\ from\ C_{RH}\ to\ S_{Mo}$. The bonds were $S_{Mo}-H_{RH}\ (S-H), C_{CRH}-H_{RH}\ (C-H), O_{Mo}-C_{CRH}\ (O-C), Mo-O_{Mo}(Mo-O), Mo=S_{Mo}(Mo-S)\ and\ Mo-(S_{Pterin})_{\beta}\ [(Mo-(B)],\ \ Mo-(S_{Pterin})_{\alpha}\ [(Mo-(F)]\ and\ \ Mo\equiv O\ (Mo-OXO)$

Deprotenated formaldehyde								
$S-H(\text{Å})$	$S_{Mo}-H_{CRH}$	$C_{CRH}-H_{CRH}$	$O_{eq}-C_{CRH}$	$Mo-O_{eq}$	$Mo-S_{Mo}$	$Mo-S_{\beta}$	$Mo-S_{\alpha}$	$Mo-O_{Apical}$
1.34999	1.34999	1.10366	1.28720	0.12500	2.26966	2.61184	2.61092	1.73904
1.51975	1.51975	1.10283	1.28838	1.76262	2.26893	2.60911	2.61101	1.73894
1.68951	1.68951	1.10633	1.29067	1.76509	2.26591	2.60887	2.61040	1.73864
1.85927	1.85927	1.11144	1.29387	1.76551	2.26629	2.60653	2.60941	1.73851
2.02903	2.03921	1.11978	1.55963	1.76487	2.26653	2.60225	2.60901	1.73835
2.19879	2.19879	1.19643	2.63477	1.89411	2.25241	2.54107	2.52109	1.72355
2.36855	2.36855	2.79162	2.65524	2.14173	2.35394	2.46416	2.46300	1.71131
2.53831	2.53831	2.74533	2.69386	2.15645	2.40619	2.45014	2.45324	1.71053
2.70807	2.70807	2.73237	2.86750	2.16885	2.45069	2.43973	2.44511	1.71011
2.87783	2.87783	2.74116	2.88796	2.17716	2.47952	2.43346	2.43974	1.70998
Protonated formaldehyde								
$S-H(\text{Å})$	$S_{Mo}-H_{CRH}$	$C_{CRH}-H_{CRH}$	$O_{eq}-C_{CRH}$	$Mo-O_{eq}$	$Mo-S_{Mo}$	$Mo-S_{\beta}$	$Mo-S_{\alpha}$	$Mo-O_{Apical}$
1.3501	1.3501	3.42942	1.21653	2.29450	2.46115	2.37241	2.38752	1.71697
1.5485	1.5485	2.66807	1.22126	2.26166	2.42307	2.38288	2.40609	1.71169
1.7469	1.7469	1.22090	1.35014	1.99852	2.25387	2.45177	2.45239	1.71229
1.9453	1.9453	1.16094	1.37261	1.98093	2.23013	2.46288	2.46009	1.71402
2.1437	2.1437	1.13630	1.38428	1.98282	2.20032	2.45595	2.49182	1.71673
2.3421	2.3421	1.11597	1.38762	1.97860	2.19026	2.45657	2.50571	1.71790
2.5405	2.5405	1.11035	1.39013	1.97796	2.18682	2.46165	2.50756	1.71832
2.7383	2.7383	1.10728	1.39195	1.97732	2.18497	2.46516	2.50980	1.71865
2.9373	2.9373	1.10551	1.39253	1.97734	2.18421	2.46804	2.51119	1.71868
3.1357	3.1357	1.10446	1.39282	1.97807	2.18386	2.47052	2.51183	1.71867
Deprotenated acetaldehyde								
$S-H(\text{Å})$	$S_{Mo}-H_{CRH}$	$C_{CRH}-H_{CRH}$	$O_{eq}-C_{CRH}$	$Mo-O_{eq}$	$Mo-S_{Mo}$	$Mo-S_{\beta}$	$Mo-S_{\alpha}$	$Mo-O_{Apical}$
1.358370	1.358370	2.89735	1.29062	2.16337	2.48203	2.43666	2.43867	1.71060
1.567373	1.567373	2.89019	1.29202	2.15347	2.44340	2.44489	2.44593	1.71074
1.776373	1.776373	2.95136	1.29499	2.13769	2.38227	2.45931	2.45795	1.71132
1.985390	1.985390	1.20872	1.55747	1.89964	2.24932	2.54576	2.52967	1.72592
2.194390	2.194390	1.12657	3.04393	1.76459	2.26728	2.60621	2.60991	1.73912
2.403390	2.403390	1.11642	3.05556	1.76483	2.26628	2.60618	2.61357	1.73933
2.612390	2.612390	1.11117	3.07976	1.76489	2.26592	2.60919	2.61304	1.73947
Protonated acetaldehyde								
$S-H(\text{Å})$	$S_{Mo}-H_{CRH}$	$C_{CRH}-H_{CRH}$	$O_{eq}-C_{CRH}$	$Mo-O_{eq}$	$Mo-S_{Mo}$	$Mo-S_{\beta}$	$Mo-S_{\alpha}$	$Mo-O_{Apical}$
1.35837	1.35837	3.16511	1.23398	2.24652	2.53991	2.39428	2.37548	1.70448
1.45438	1.45438	3.14735	1.23398	2.24406	2.52764	2.39600	2.37694	1.70441
1.55438	1.55438	3.12425	123405	2.24132	2.50946	2.39873	2.37891	1.70431
1.65438	1.65438	1.29772	1.33362	2.01525	2.27545	2.44769	2.44383	1.71131
1.75438	1.75438	1.21924	1.35805	1.99553	2.24842	2.45504	2.45341	1.71301
1.85438	1.85438	1.18220	1.37183	1.98474	2.23364	2.45999	2.45945	1.71409
1.95438	1.95438	1.16002	1.38600	1.97805	2.22432	2.46306	2.46446	1.71479

2.25438	2.25438	1.12860	1.39365	1.96879	2.21115	2.46903	2.47414	1.71539
2.65438	2.65438	1.11610	1.40042	1.96409	2.20754	2.47497	2.47991	1.71466
Deprotenated propylaldehyde								
$S-H(\text{Å})$	$S_{Mo}-H_{CRH}$	$C_{CRH}-H_{CRH}$	$O_{eq}-C_{CRH}$	$Mo-O_{eq}$	$Mo-S_{Mo}$	$Mo-S_{\beta}$	$Mo-S_{\alpha}$	$Mo-O_{Apical}$
1.349999	1.350000	2.91419	1.28746	2.16671	2.48290	2.43607	2.43602	1.71028
1.574106	1.574110	2.89625	1.28924	2.15692	2.44194	2.44436	2.44390	1.710461
1.798213	1.798210	2.94916	1.29276	2.13963	2.37594	2.46029	2.45670	1.71110
2.022320	2.022320	1.20553	1.53339	1.90574	2.24553	2.54410	2.52572	1.72519
2.246427	2.246430	1.12238	3.00852	1.76520	2.26711	2.60480	2.60966	1.73897
2.470534	2.470530	1.11352	3.04353	1.76549	2.26614	2.60572	2.61270	1.73918
2.918748	2.918750	1.10717	3.09997	1.76514	2.26606	2.60987	2.61292	1.73945
Protonated propylaldehyde								
$S-H(\text{Å})$	$S_{Mo}-H_{CRH}$	$C_{CRH}-H_{CRH}$	$O_{eq}-C_{CRH}$	$Mo-O_{eq}$	$Mo-S_{Mo}$	$Mo-S_{\beta}$	$Mo-S_{\alpha}$	$Mo-O_{Apical}$
1.31439	1.31439	3.19228	1.23535	2.24715	2.54128	2.39676	2.37481	1.70404
1.41439	1.41439	3.17997	1.23536	2.24477	2.53110	2.39829	2.37606	1.71043
1.51439	1.51439	3.19795	1.23301	2.24505	2.44064	2.44092	2.38796	1.70398
1.61439	1.61439	1.40390	1.30926	2.03841	2.30123	2.44165	2.43498	1.70341
1.71439	1.71439	1.24105	1.34993	2.00484	2.25591	2.45377	2.44919	1.71242
1.81439	1.81439	1.19453	1.36642	1.99098	2.23816	2.45865	2.45696	1.71370
1.91439	1.91439	1.16800	1.37686	1.98242	2.22270	2.46194	2.46264	1.71452
2.01439	2.01439	1.15090	1.38394	1.97681	2.21933	2.46451	2.46717	1.71506

Appendix – IV: The raw data for the Total Energies Difference at C – H, TS and S – H in the linear transit calculation

Table – 4: Total Energy difference for formaldehyde, acetaldehyde and propylaldehyde substrates bound to the active site. It was developed from the Table – 1: A-I

Structure	S-H (In Angstrom)	Energy$(Kcal/mol)$
Protonated Formaldehyde	3.13570	-1056670.443
	1.60824	-1056661.232
	1.35010	-1056672.242
Deprotenated Formaldehyde	2.87783	-1056247.819
	2.03921	-1056234.786
	1.34999	-1056278.305
Protonated Acetaldehyde	1.65438	-1081330.309
	1.65438	-1081343.029
	1.35837	-1080910.143
Deprotenated Acetaldehyde	2.61239	-1090910.143
	1.98539	-1080892.711
	1.35837	-1080935.313
Protonated Propylaldehyde	2.01439	-1105995.760
	1.61439	-1105988.400
	1.31439	-1106012.727
Deprotenated Propylaldehyde	2.918748	-1105581.793
	2.022320	-1105565.163
	1.349999	-115607.334

Appendix – V: The raw data for the Mechanism of the Reductive Half Reaction of Xanthine Oxidase

Table – 7: Total Energies for optimized geometries of protonated and deprotenated formaldehyde and corresponding product bound to xanthine oxidase active site through hydroxide oxygen. The calculation were performed on geometries from (a) to (g) of schematic diagram for figure – 13:

(a) Before substrate bound (b). Substrate bound complex (c). Tetrahedral transition state complex (d). Product bound with oxidation stat Mo IV (e). Product bound with Mo V (SH) (f). Product bound with MO V (S), (g). Product release In which the value in (g) is -46858.7, for the deprotenated approximate to -220.71824 and -47224.2, and for the protonated approximate is -224.2007

Deprotenated formaldehyde		
Structure	**Total Energy $(Kcal/Mol)$**	**Normalized Energy $(Kcal/Mol)$**
(a)	$\mathbf{-1056635.366}$	**0.0000000**
(b)	$\mathbf{-1056228.770}$	**406.5957148**
(c)	$\mathbf{-1056217.907}$	**417.4584938**
(d)	$\mathbf{-1056261.492}$	**373.8735360**
(e)	$\mathbf{-1056294.643}$	**340.7226482**
(f)	$\mathbf{-1055882.041}$	**753.3249823**
(g)	$\mathbf{-1103494.084}$	$\mathbf{-220.7182400}$

Protonated formaldehyde		
Structure	Total Energy $(Kcal/Mol)$	Normalized Energy $(Kcal/Mol)$
(a)	-1056635.366	0.00000000
(b)	-1056653.604	-18.23778550
(c)	-1056641.849	-6.48333000
(d)	-1056650.423	-15.05749000
(e)	-1056602.491	32.87451125
(f)	-1056280.983	354.38271480
(g)	-1103859.566	-224.20070000

REFERENCES:

1. Stiefel E.L. (1973) Proposed molecular mechanism for the action of molybdenum in enzymes: "*Coupled proton and electrons transfer" Proc. Nat. Acad. Sci. -70(4) pp 988-992*
2. Hille R. (1999) Molybdenum Enzymes *Essays Biochem. 34 pp (125 -137)*
3. Hille R. (2003) Molecular Molybdenum Enzymes *Chem. Rev. 96 pp (2757 – 2816*)
4. Gangeswaran R., Lowe D.J., and Eady R.R. (1993) Purification and characterization of the assimilatory nitrate reductase of Azotobacter *Vinelandii J. Biochem*. 289 pp (355-342)
5. Cabello P., Roldan M.D., and Moreno – Vivian C. (2004) *Nitrate reduction and the nitrogen cycle in archea Microbiology 150 pp (3527 – 3546)*
6. Richert D.A and Westerfield W.W. (1954) *The relationship of iron to xanthine oxidase J. Biochem 209 pp (179 – 189)*
7. Enroth C., Eger B.T., Okamoto T., Nishino T., and Pai E.F. (2000) *Crystal structures of bovine milk xanthine dehydrogenize and xanthine oxidase: Structure based mechanism of conversion. Proc. Nat. Acad. Sci. 97 pp (10723 – 10728)*
8. Kisker C, Schindelin H. and Rees C.D. (1997) *Molybdenum cofactor containing enzymes: Structure and mechanism. Annu. Rev. Biochem. 66 pp (233- 267)*
9. Nishino T. (1994) *the conversion of xanthine dehydrogenize to xanthine oxidase and the role of the enzyme in reperfusion injury J. Biochem. 116(1) pp (1 – 6)*
10. Pauff J.M. and Hille R. (2009) *Inhibition studies of bovine xanthine oxidase by luteolin, silibrinin, quercetin, and curcumin J. Nat. prod. 72 (4) pp (725 – 731)*
11. Delia C.E. and Stripe F (1968) *The regulation of xanthine oxidase in rat liver: Modification of the enzyme activity of rat liver supernatant on storage at* $-20℃$, *J. Biochem. 108 pp (349 – 351)*

12. Waud W. R and Rajagopalan K.V. (1976). *Purification and properties of the NAD^+ dependent (Type D) and O_2 dependent (Type O) forms of rat liver xanthine dehydrogenize Arch. Biochem. Biophy 172 pp (354 – 364)*
13. Harrison R. (2002) *Structure and function of xanthine oxidereductase: Where are we now? Free radical biology & Medicine 33 (6) pp (774 – 797)*
14. Ichida K., Amaya Y., kamathani N., Nishino T., Hosoya T. and Sakai O. (1997) *identification of two mutations in human xanthine dehydrogenize gene responsible for classical type I xanthine J. Clin. Invest.99 (10) pp (2391 – 2397)*
15. Berry C.E. and Hare J.M. (2004) *Xanthine oxidereductase and cardiovascular disease: Molecular mechanism and pathophysiological implications. J. physiol. 555 (3)*
    pp (589 – 606)
16. Harrison R. (2006) *Milk xanthine oxidase: Properties and physiological roles. J. int. Dairy. 16 pp (546 – 554)*
17. Linder N., Rapola J., Raivio K.O. (1999) *Cellular expression of human xanthine oxidereductase protein in normal human tissues. Lab. Invest. 79 pp (967 – 974)*
18. Ball E.G. (1939). Xanthine oxidase: *Purification and Properties*
    J. Biochem. 128 pp (51 – 67)
19. Bray R.C. and Meriwether L (1966) *Electron spin resonance of xanthine oxidase substituted with molybdenum 99 Natur. 212 pp (467 – 469)*
20. Eger B.T., Okamoto K., Enroth C., Sato M., Nishino T., and Pai E.F. (2000) *Purification crystallization and preliminary X - Ray diffraction studies of xanthine dehydrogenize and xanthine oxidase isolated from bovine milk. Acta Crystollographica D56, pp (1656- 1658)*
21. Harris C.M. and Massey V. (1997). *The oxidative half reaction of xanthine dehydrogenize with NAD: Reaction kinetics and steady state mechanism J. Biochem. 272 pp (28335 – 28341)*
22. Stokert A.L., Shinde S.S., Anderson R.F., and Hille R. (2002). *The reaction mechanism of xanthine oxidase: Evidence for two electrons chemistry rather than sequential one electron steps. J. Am. Chem. Soc. 124 pp (14554 – 14555)*
23. Massey V., Brumby P.E., Komai H. Palmer G. (1969) *Studies on milk xanthine oxidase: Some spectral and kinetic properties. J. Biochem. 244 pp (1682 – 1691)*

24. Olson S.J., Ballou P. D., Palmer G., and Massey V. (1994): *The mechanism of action of xanthine oxidase family of molybdenum enzymes. J. Biochem. 249 (14) pp (4363 – 4382)*
25. Huber R., Hof P., Duarte R.O., Moura J.J. G., Moura I., Liu M.Y., LeGall J., Hille R., Archer M., and Romao M.J. (1996) *A structure based catalytic mechanism for the xanthine oxidase family of molybdenum enzymes. Proc. Nat. Acad. Sci. USA 93 pp (8846 – 8851)*
26. Hille R. and Massey V. (1981) *Studies on the oxidative half reaction of xanthine oxidase J. Biochem. 256 (17) pp (9090 – 9095)*
27. Xia M., Dempski R., and Hille R. (1999). *The reductive half reaction of xanthine oxidase: Reaction with aldehyde substrates and identification of the catalytically labile oxygen. J. Biochem. 274 pp (3323 -3330)*
28. Voittyuk A.A., Albert K., Romao M.J., Huber R., and Roesch N. (1998). *Substrate oxidation in the active site of xanthine oxidase and related enzymes: A model density functional study. Inorg. Chem. 37 (2) pp (176 – 180)*